Mémoire, Partim B

Auteur : Bastiaens, Quentin
Promoteur(s) : Quinton, Loïc
Faculté : Faculté des Sciences
Diplôme : Master en sciences chimiques, à finalité approfondie
Année académique : 2023-2024
URI/URL : http://hdl.handle.net/2268.2/20035

FACULTY OF SCIENCES
Chemistry Department

Mass Spectrometry Laboratory – Prof. Quinton Loïc

Combining mass spectrometry imaging and LC-MS/MS experiments for investigating the metabolome of arthropods
Case study: *Steatoda nobilis*

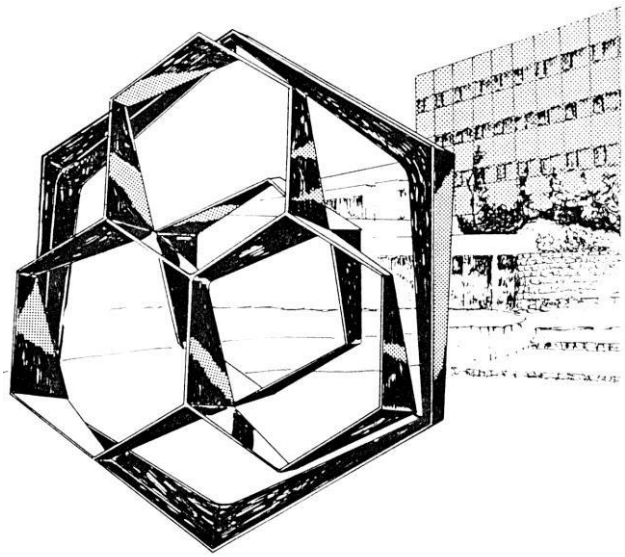

Academic year 2022-2023

Dissertation submitted by
Quentin BASTIAENS
for the fulfilment of the degree of
Master in Chemistry

Contents

Abbreviation table

α-cyano-4-hydroxycinnamic acid	CHCA (or HCCA)	N,N-dimethylaniline	DANI
Aniline	ANI	Nicotinamide adenine dinucleotide (oxidized form)	NAD
Ceramide phosphatidylinositol	PI-Cer	Nicotinamide adenine dinucleotide (reduced form)	NADH
Ceramide phosphatidylethanolamine	PE-Cer	Nicotinamide adenine dinucleotide phosphate (reduced form)	NADPH
Desorption ElectroSpray Ionization	DESI	Nuclear magnetic resonance	NMR
2,5-Dihydroxybenzoic acid	DHB	Part per million	ppm
Diglyceride	DG	Phosphatidylcholine	PC
ElectroSpray Ionization	ESI	Phosphatidylethanolamine	PE
Fourier-Transform Ion-Cyclotron Resonance Mass spectrometry	FT-ICR MS	Phosphatidylglycerol	PG
Galactosylsylceramide	GalCer	Phosphatidylinositol	PI
Gigabyte	GB	Phosphatidylinositol bisphosphate	PIP
Glucosylceramide	GlcCer	Phosphatidylserine	PS
Glycerolceramide	GlyCer	Phosphatidic acids	PA
High-Performance Liquid Chromatography	HPLC	Secondary ion/neutral mass spectrometry	SIMS/SNMS
Inositol phosphoceramide	IPC	Sphingomyelin	SM
Laser Desorption/Ionization	LDI	Sulfoquinovosyl diglyceride	SQDG
Liquid chromatography	LC	Terabyte	TB
Lysophosphatidylcholine	LysoPC	Time Of Flight	TOF
Mass spectrometry	MS	Trapped Ion Mobility Spectrometry	TIMS
Mass Spectrometry Imaging	MSI	Trifluoroacetic acid	TFA
mass-to-charge ratio	m/z	Triglyceride	TG
Monoacyl phosphatidylcholine	LPC	Ultra-High-Performance Liquid Chromatography	UHPLC
Monoglyceride	MG		

Acknowledgements

I would like to thank my promoter, Prof. Loïc Quinton, for welcoming me in the laboratory and for this subject which was captivating and enriching. I also want to thank him for his expertise, his precious advice and his guidance during my thesis.

I also want to thank Dr. John Dunbar for bringing the samples of *Steatoda nobilis* directly from Ireland to our laboratory and for his invaluable contribution to my understanding of the spider.

The master thesis is quite an experience and can be quite frustrating sometimes, so I would like to thank my supervisors Damien Redureau and Dr. Virginie Bertrand, for their feedback and for their contributions to this project. I also want to thank them for their insightful comments during the thesis and for their guidance while navigating the complexity of my subject.

My thanks also go to Dr. Johann Far and Pierre Burguet for their help for the data acquisition in ion mobility mass spectrometry and mass spectrometry imaging. I am also grateful to Dr. Christopher Kune for his help with the analysis of mass spectrometry data analysis.

I would also like to thank the members of the reading committee, respectively Prof. Loïc Quinton, Prof. Christian Damblon, Dr. Virginie Bertrand and Dr. Damien Sluysmans for agreeing to evaluate my work.

Then, I would like to offer my special thanks to the entire MSLab team, and in particularly to the “biology” and “omics” platform: Lou, Fernanda, Thomas C., Thomas T., Dominique, Gabriel and Maximilien. But also, to Nancy and Lisette, Cedric D. and Zeina for their advice.

I also have to thank the mémorants of the MSLab, Maxime, Bastien, Charles, Vincent, Simon and Matthieu, for the fun times in the lab and for making this master thesis unforgettable.

My last thanks go to all those who have contributed in one way or another to the success of this work. Thanks to my family and friends for helping me throughout my academic journey at the university.

Abstract

The noble false black widow spider, *Steatoda nobilis*, is an invasive species widely observed in Europe, and whose venom has recently been demonstrated to be of concern. Indeed, by adapting easily to urban environments, spider bites can cause significant effects, even in humans. The purpose of this work is to investigate the nature and localization of *Steatoda nobilis* metabolites so as to better describe the spider, especially since the metabolome of arthropods is currently understudied. In this study, we propose an experimental protocol for preparing whole spider samples. Initially, extracts will be performed and analyzed by LC-MS/MS using a TIMSTOF-pro-2 type mass spectrometer. Subsequently, spider sections will be prepared for imaging using an FT-ICR type spectrometer. The goal is to identify metabolites using different mass spectrometry methods and then locate these molecules on sections to determine their organ/zone of origin through imaging.

Sample preparation, whether for LC-MS/MS or imaging, is challenging for such complex samples. To be analyzed by LC-MS/MS, spiders must first be crushed, and metabolites extracted from this mash. The sample must still be treated with care to ensure that no particles that could obstruct the chromatographic system persist in the liquid sample. For imaging, spiders will be embedded in a gel, cryogenically frozen, sliced into thin sections, and coated with matrix for observation by MALDI-FT-ICR. Besides the analytical approach demonstrating the complexity of the *Steatoda nobilis* metabolome, the LC-MS/MS results will be exploited to confirm the identification of ions obtained in imaging.

Mass spectrometry imaging is a complex method to implement, generating very large data files, up to several Tb. Data processing involves reducing their size by controlled downsizing of the acquired data quantity. The images will be studied using a combination of three bioinformatics tools: (i) SCiLS® to assess image quality and transform files into open-source formats; (ii) a laboratory-developed program to classify ions by the Kendrick method and link them to specific spider organs, and (iii) Metaspace® to identify molecules and link them to previously highlighted areas. One challenge of this approach will be the lack of data in the databases on which identification can rely.

In conclusion, the combination of these two analytical methods yields promising results for the metabolomic study of whole specimens of *Steatoda nobilis*. It is evident that both approaches are complementary and could form a credible basis for the study of metabolomes of arthropods, insects, or any other small-sized animal that has been overlooked until now.

Résumé

La fausse veuve noire, *Steatoda nobilis*, est une espèce d'araignée invasive observée abondamment en Europe et dont le venin a été récemment démontré préoccupant. En effet, s'adaptant facilement aux milieux urbains, les morsures de l'araignée peuvent provoquer des effets importants, même chez humains. Le but de ce travail est d'investiguer la nature et la localisation des métabolites de *Steatoda nobilis* afin de mieux la décrire, mais surtout car le métabolome des arthropodes est actuellement peu, si ce n'est pas, étudié. Dans ce travail, nous proposons un protocole expérimental pour préparer des échantillons d'araignées entières. Dans un premier temps, des extraits seront effectués puis analysés par LC-MS/MS, par l'intermédiaire d'un spectromètre de type TIMSTOFpro-2. Dans un second temps, des coupes d'araignée seront effectuées afin de les imager à l'aide d'un spectromètre de type FT-ICR. Le but de ce travail est d'identifier les métabolites avec l'aides des différentes méthodes de spectrométries de masse puis de localiser ces molécules sur les coupes à pour savoir de quel organe/zone elles proviennent, grâce à l'imagerie.

La préparation d'échantillons, que ce soit pour la LC-MS/MS ou pour l'imagerie, est assez périlleuse pour des échantillons aussi complexes. Pour pouvoir être analysées par LC-MS/MS, les araignées doivent être tout d'abord broyées et les métabolites extraits de ce broyat. L'échantillon devra encore être traité avec soin afin de s'assurer qu'aucune particule susceptible d'obstruer le système chromatographique ne persiste dans l'échantillon liquide. Pour l'imagerie, les araignées seront inclues dans un gel puis cryogénisées, afin d'être sectionnées en fines coupes puis recouvertes de matrice pour pouvoir être observées par MALDI-FT-ICR. Outre l'approche analytique permettant de montrer la complexité du métabolome de *Steatoda nobilis*, les résultats obtenus en LC-MS/MS seront exploités afin de confirmer l'identification des ions obtenue en imagerie.

L'imagerie par spectrométrie de masse est une méthode assez complexe à mettre en place, générant de plus des fichiers de données très volumineux, jusque plusieurs Tb. Le traitement de données impose de passer par une étape de réduction de leur taille, en diminuant de manière contrôlée la quantité de données acquise. Les images seront étudiées via une combinaison de trois outils bioinformatiques : (i) SCiLS® pour évaluer la qualité des images et transformer les fichiers en formats open-source ; (ii) un programme développé au laboratoire afin de classer les ions par la méthode de Kendrick et les lier à des organes particuliers de l'araignée et (iii) Metaspace® afin d'identifier les molécules et les lier aux zones précédemment mises en évidence. Nous verrons que l'une des difficultés de cette approche résidera dans le manque de données présentes dans les banques de données sur lesquelles l'identification peut se baser.

En conclusion, La combinaison de ces deux méthodes analytiques donne des résultats prometteurs pour l'étude métabolomique de spécimen entier de *Steatoda nobilis*. Il apparait comme assez évident que les deux approches sont complémentaires et pourrait constituer une base crédible pour l'étude de métabolomes d'arthropodes, d'insectes ou de tout autre animal de taille restreinte et jusqu'alors ignoré.

I. Introduction

A. *Steatoda nobilis, an invasive European spider*

The false noble widow, *Steatoda nobilis* (Figure 1), is a spider that belongs to the family of the true widow spiders (Theridiidae). Despite not being part of the same genus, they remain closely related. Indeed, the true and false widow spiders respectively belong to the *Latrodectus* and the *Steatoda* genus. *Steatoda nobilis* originates from the Macaronesian archipelago but has recently been spotted all around the world. This species started invading many countries in the last hundred years, which has an important impact on the United Kingdom and Ireland societies due to a significant increase in their number present in their territories (Dugon *et al.*, 2017). Many Theridiids live in synanthropic habitats which means in man-made structures such as in houses, parks but also schools and playgrounds. They are not found in the uninhabited countryside, in caves or even in forests.

Figure 1. Photo of a male (left) and female (right) *Steatoda nobilis*. Image taken nhm.ac.uk

Steatoda nobilis has a faster reproduction cycle than most spider species on the planet. It reproduces more often, once per month, and produces more eggs per egg sac (35 to 200) than other species. They also live up to 5 years which is far longer than the local endemic spiders, such as *Zygiella x-notata* that only lives 1 year. They can also reproduce in winter, while most spiders tend to wait for warmer days to produce eggs again (Dugon *et al.*, 2017; Rayner *et al.*, 2022). Additionally, to the fact that the population of S. *nobilis* increases quite rapidly, this spider also impacts the local spider species in Ireland because of their aggressivity and their powerful venom. Indeed, studies showed if other spiders try to share the same area as *S. nobilis*, the main response of the spider is to attack and this usually results in the death of the other spiders (Rayner *et al.*, 2022). Since this species has a rapid expansion, adapts rapidly to many biotopes, positively competes for the territory of other spiders and kills them if it feels threaten, *Steatoda nobilis* can be classified as one of the most invasive species on the planet (Bauer *et al.*, 2019). If we add the fact that it lives in close contact with human beings, this leads to an increase in the risk of human envenomation since encounters become more likely.

This spider preys on small invertebrates like Woodlice (subphylum *Crustacea*) and other spiders (Dugon *et al.*, 2017). It has been reported that a lizard was killed by their venom (Rayner *et al.*, 2022), a pygmy shrew (*Sorex minutus*) as well (Dugon *et al.*, 2023), and pipistrelle bats (Dunbar *et al.*, 2022). This shows that the spider can undoubtedly kill insects, crustaceans but also mammals and reptiles with its venom. Therefore, the main concern is that the *Steatoda* family (and especially *S. nobilis*) possesses a powerful venom with potent toxins that can represent a threat to human health. In the case of humans, the main symptoms are severe pain, swelling, inflammation (Bauer *et al.*, 2019; Dugon *et al.*, 2017) and necrosis (Dunbar *et al.*, 2022b, 2022a). These symptoms are also common with the bite of Theridiidae spiders and last a few days. This is more problematic for children and babies who might suffer from more severe symptoms due to their lower body mass, since the same quantity of toxins can be transferred to an adult or a child. Dunbar *et al.* also noticed that some species of bacteria could live and proliferate on the fangs of spiders. These bacteria can infect humans once they are bitten by the spider which, in addition to the symptoms of the bite, can cause a serious infection lasting far longer than the usual envenomation symptoms (Dunbar *et al.*, 2022a). Moreover, some of these bacteria are resistant to antibiotics, which results in untreatable infections that can last for a long time (up to 6 months) and leave permanent damage to the victim. As *Steatoda nobilis* additionally lives in close quarters to humans and reproduces fast, there will be an increase in the number of encounters as time goes by and more risk of people getting severely ill or injured due to a bite. So, there is a need to study this species to further understand how it functions, to try to limit its uncontrolled rapid expansion and what we can do to prevent bites or treat them once a human gets bitten.

A recent study, conducted through a collaboration between the National University of Galway and the University of Liège, focused on the characterization of the venom of *S. nobilis*, aiming at understanding why the venom was so potent and to understand its toxic effects (Dunbar *et al.*, 2020). They discovered that the venom contained substantial amounts of α-latrotoxins as well as other similar proteins such as latrocrustotoxins targeting crustaceans and α-latroinsectotoxins meant to kill insects. Such toxin classes are commonly found in true widow spider venoms and are known for being powerful toxins. The most interesting ones for humans are the α-latrotoxins since they are targeting vertebrates. α-latrotoxins are neurotoxins that seems to function as homotetramers to form pores on the surface of presynaptic membrane of nervous cells (Figure 2) (Chen *et al.*, 2021). These pores are calcium pores which induces an afflux of Ca^{2+} inside the cell membrane. It is known that Ca^{2+} causes the release of the neurotransmitters present in the vesicles of the synapse, but the deep mechanism of action of the α-latrotoxin is still not well known (Yan *et al.*, 2015). The fact this spider has a venom that can kill vertebrates is quite surprising since its diet is composed of insects, crustaceans and other arachnids. *Steatoda nobilis* venom can be used to defend itself against aggressions from small animals that might attack it, but the potency of the α-latrotoxin seems disproportionate for a defensive purpose. The study of the venom was done on several female spiders (Dunbar *et al.*, 2020), but male venom composition was not published so far (*ongoing study*).
Even if the venom composition of female *Steatoda nobilis* venom is known, no additional information is known so far at the molecular level for this spider. One of the objectives of this master thesis is to provide insights into the metabolome of the spider. Indeed, arachnid's metabolomes have never been described so far and we want to produce the first investigation in such metabolomes.

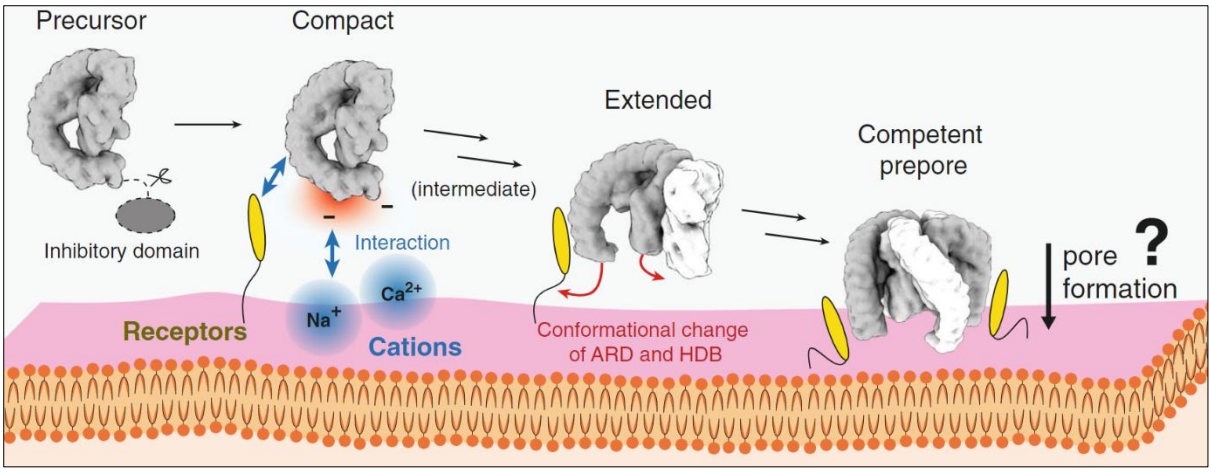

Figure 2. Proposed model of latrotoxin action at the presynaptic membrane prior membrane insertion. Image taken from (Chen *et al.*, 2021)

B. Metabolomics: what, why and how.

Metabolites are low molecular weight bioorganic molecules that are present in every organism on the planet. The chemical nature of metabolites and their concentration is dependent on the organism's physiological, pathological, and biochemical status, and can provide information on the lifestyle and health of the target. Metabolites can be separated in two large families: the primary metabolites that play an important role in the growth, the development and the reproduction of the organism, and secondary metabolites which are all the metabolites which are not considered as primary metabolites. Metabolites can also be separated into different structural classes which include amino acids, carbohydrates, nucleotides, lipids, coenzymes, and cofactors. Amino acids play a key role in the structure and physiology of organisms, nucleotides are the base of the ADN and ARN for all living beings, carbohydrates are a source of energy for organisms to function, cofactors and coenzymes are used by organisms for enzymatic activities and the main roles of lipids include storing energy, signalling, or transferring information, and are used in the structure components of cell membranes.

The study of the metabolome of an organism is an old technique that can be traced to ancient China. But the idea that the metabolites of individuals are distinct and that the "metabolic pattern" can be "fingerprinted" dates from the late 1940s with Williams *et al.* (Nagana Gowda & Djukovic, 2014; Ren *et al.*, 2018). There are two main techniques to study metabolites: mass spectrometry (MS) and nuclear magnetic resonance (NMR). The first "metabolomic" study by mass spectrometry was performed by Horning *et al.* in 1971 while in NMR, the first interest in metabolomics rose after Bales *et al.* investigations who demonstrated the use of the technique for the diagnosis of diabetes (Bales *et al.*, 1984). (Nagana Gowda & Djukovic, 2014; Ren *et al.*, 2018).

In the context of our study where the samples are complex and are supposed to contain hundreds to thousands of different metabolites, MS appears as the best method due its property to be easily hyphenated to separation techniques such as capillary electrophoresis or liquid chromatography, but also due to its speed of analysis, its high sensitivity and mass accuracy. The main asset of MS is to be able to detect, quantify and elucidate the structures of the entire sample in one analysis. Although at the time of this study, obtaining all that information for a sample is very challenging.
As explained before, the family of metabolites is composed of a wide class of molecules which possess variable physical and chemical properties. In a single organism, these metabolites are additionally

expressed in various concentrations. It is therefore utopian to search for an analytical approach that would provide an exhaustive overview of such a metabolome. The other major issue when performing metabolomics on whole animals with MS, is that the sample is usually too complex to be immediately sent for analysis. Thus, purification and separation techniques, such as gas and liquid chromatography, are usually mandatory to make the analysis possible. Once separated, the sample is studied in MS in a process described in the "mass spectrometry" section below.

When the study does not target the volatile metabolites, liquid chromatography and mass spectrometry are, in parallel to NMR, the most powerful analytical techniques to perform metabolomics measurements. Coming back to our topic, it appears then that metabolomics investigation of *Steatoda nobilis* could be efficiently achieved by a coupling between liquid chromatography and mass spectrometry (LC-MS/MS). This will constitute the first part of this project. However, this approach would give access to a global overview of the spider metabolome. To go deeper into this investigation, the localization of the metabolites in the spider organs would be valuable. To reach this goal, mass spectrometry imaging (MSI) can be used (Gao *et al.*, 2022) and its application to *Steatoda nobilis* spiders will constitute the second main part of this present master thesis.

C. Liquid chromatography and mass spectrometry: the duo of choice for metabolome investigations.

Liquid chromatography (LC). LC is a separation method that rests on the difference of affinity of molecules, such as metabolites, between a liquid mobile phase and a solid stationary. The molecules are injected in the flow of the mobile phase that crosses a column containing a solid stationary phase, usually silica modified (grafted) bead or monolithic polymers. The nature of the stationary phase, and of the mobile phase as well, must be chosen in function of the type of compounds to be separated. The molecules crossing the column interact differently with the solid phase depending on the difference of affinity for it and for the mobile phase. The ones with a high affinity for the stationary phase will take longer to go through the column, while molecules with poor affinity will go more rapidly straight through the column. At the end of the column, the molecules are separated spatially, and they get out of the column at different retention times (Snyder *et al.*, 1979). An issue may occur if several molecules have almost the same affinities for the stationary and the mobile phases. In that case, the molecules coelute in the same chromatographic peak and are therefore not separated. To counter this problem, High-Performance Liquid Chromatography (HPLC) then Ultra-High-Performance Liquid Chromatography (UHPLC) were developed. UHPLC uses columns that have micrometric internal diameters (compared to millimeters for HPLC) so that the interactions between the molecules and the solid phase are substantially amplified. To ensure the liquid flows through the column high pressure pumps are required. The liquid is sent slowly (usually 1 to 2 mL/min) through the column at several thousands of psi. The increase of chromatographic resolution reached by the miniaturization of the chromatographic systems improves the separation of species who were coeluting in HPLC (Avela *et al.*, 2020; Jacob *et al.*, 2019; Macnair *et al.*, 1997; Perez de Souza *et al.*, 2021). The columns usually used for metabolomic are reverse phase column with C18 coating to be able to analyze low polarity molecules and Hydrophilic Interaction Liquid Chromatography (HILIC® columns used to analyze polar molecules (Tang *et al.*, 2016).

Mass spectrometry (MS). MS has been continuously improved since its discovery in since 1912 by J.J Thomson (Griffiths, 2008), and is now essential for the analysis of chemicals and biomolecules. Each

mass spectrometer is composed by three common functionalities/devices that are an ionization source used for producing the ions from neutral molecular species, a mass analyzer used to classify the ions according to their mass-to-charge ratio (m/z), and a detector counting the ions at each m/z and playing the role of amplifier of the signal. Indeed, as the mass measurement is based on the behavior of the molecules submitted to an electric and/or a magnetic field(s), these molecules need to be charged. Mass spectrometry is additionally made in the gas phase to amplify the effects of the electric and magnetic fields, but also to allow the molecule to be analyzed naked, without the contribution of the solvent. In summary, the analytes must be desorbed from the sample and ionized before being detected by the mass spectrometer. Both the charge and the desorption can be performed using many different techniques including electrospray ionization (ESI) and matrix assisted laser desorption/ionization (MALDI), which are used in this work and described in more detail in the next sections. The readers must keep in mind that citing these two ion sources is far from being exhaustive as many others could have been cited as well (Challen & Cramer, 2022). The analyzer will classify/detect the ions according to their m/z and send them to the detector which will detect and amplify the signal. As the charge can be calculated, the mass of the analytes/metabolites can be determined (Herbert & Johnstone, 2003). If tandem mass spectrometry (MS/MS) is performed, structural information on the studied sample can also be measured (Ahamad *et al.*, 2022; El-Aneed *et al.*, 2009).

The following section will be more focused on the description of the mass spectrometer used to perform the LC-MS/MS analysis of *Steatoda nobilis* metabolome. This spectrometer, called TIMSTOF-Pro-2 (see Material and Methods), is equipped of an ESI source and a time-of-flight (TOF) analyzer which will be now described in more detail.

Electrospray Ionization (ESI). A plethora of methods for soft ionization of biomolecules have been developed in the past decades. One can cite plasma desorption, ElectroSpray Ionization (ESI) and Matrix Assisted Laser Desorption/Ionization (MALDI) (Becker & Jakubowski, 2009; Molnar & Shelley, 2021). Electrospray ionization is however the main ionization source utilized in mass spectrometry due to its property to not only allow very large molecules to be gently ionized and detected, but also as it constitutes a perfect interface between the liquid phase eluting from liquid chromatography systems and the gas-phase needed for mass spectrometry (see above). ESI is based on the application of an electric potential difference of tens of kilovolts between a thin needle, from where the liquid phase containing the sample elutes, and the entry of the spectrometer. In positive ionization mode, the created electric attracts the positive ions toward the spectrometer, creating a so-called Taylor cone (Figure 3). At the top of the cone, the liquid emits small droplets containing solvent and analyte molecules. From there, three models exist for the ionization: the charged residues model, the ionic evaporation model and the chain ejection model (Awad *et al.*, 2015; Konermann *et al.*, 2013). In the ion evaporation model the solvent starts evaporating due to the temperature and high voltage which leads to a decrease in the size of the droplet. This effect lasts until the coulombic repulsion between the charged particles becomes too important and overcomes the surface tensions maintaining the droplet together. The threshold of this force is called the “Rayleigh limit” and after that, the droplet is ripped apart into smaller droplets. These smaller droplets then undergo the same phenomenon until a single ion is in the droplet with the solvent according to Dole’s model (Dole *et al.*, 1968). Once the solvent is evaporated, the ion is still propelled by the electric field to the mass spectrometer to be analyzed (Bleiholder *et al.*, 2006; Gomez *et al.*, 1994; Jimenez *et al.*, 2007; Kebarle *et al.*, 2000; Markert *et al.*, 2021; Myers *et al.*, 2006; Fenn *et al.*, 1984). In the case of large globular species, such as folded proteins, the charge residue model is the one that best represents the ionization process. In this model,

for nanodroplets that are Rayleigh-charged, as the solvent disappears, the charge of the vanishing droplet is transferred to the analytes. Konermann *et al.* also writes that "*charge residue model nanodroplets remain close to the Rayleigh limit throughout the entire shrinkage process, implying that the droplet sheds charge as its radius decreases. This charge reduction can take place by IEM ejection of solvated protons and small ions*" (Konermann *et al.*, 2013). However, for unfolded proteins, the chain ejection model reflects the ionization process better than the other two models. For this model, since the unfolded protein is still in a Rayleigh-charged nanodroplets, the hydrophobic part of the protein is unstable and will migrate to the surface of the droplet before being expelled to the gas phase. The rest of the protein is then slowly separated from the solvent but will retain the charge of the droplet (Konermann *et al.*, 2013).

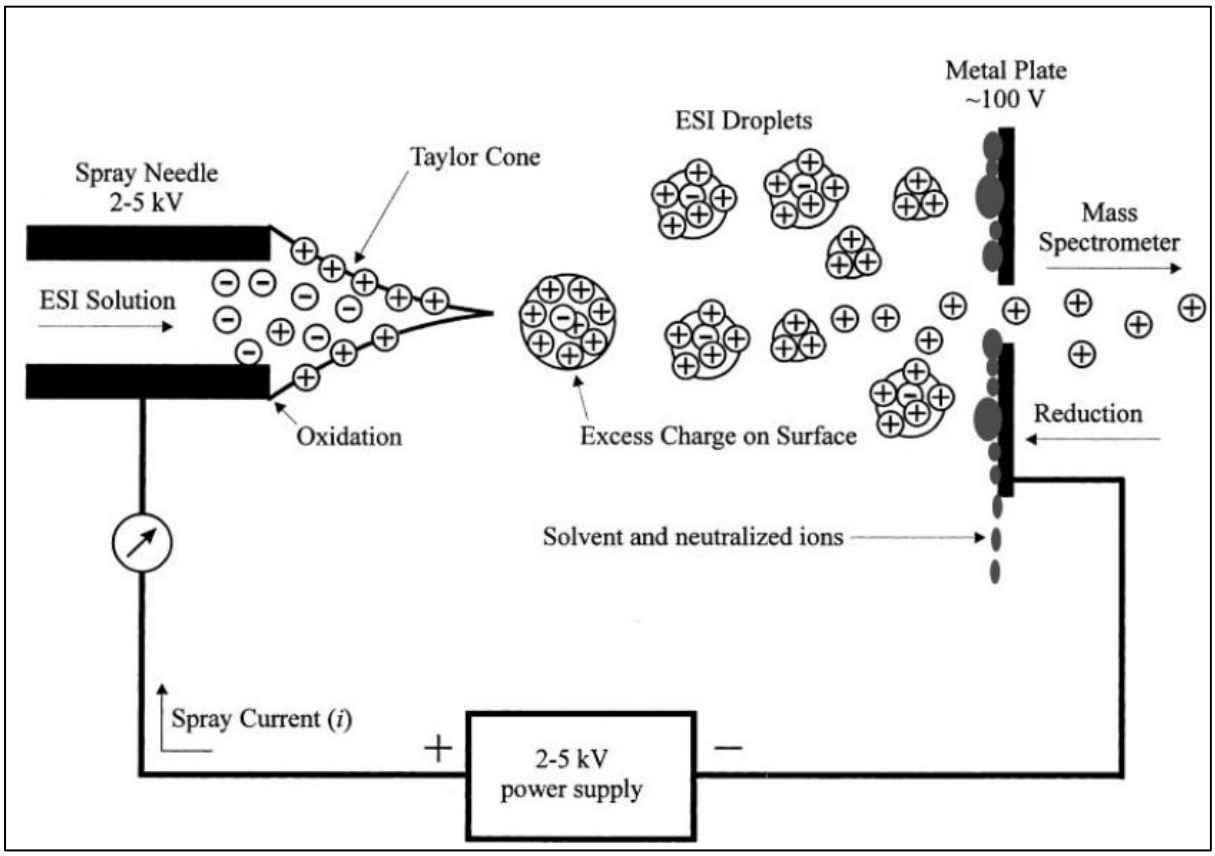

Figure 3. Schematic of the electrospray ionization process. The analyte solution is pumped through a needle to which a high voltage is applied. A Taylor cone with an excess of positive charge on its surface forms as a result of the electric field gradient between the ESI needle and the counter electrode. Charged droplets are formed from the tip of the Taylor cone, and these droplets evaporate as they move towards the entrance to the mass spectrometer to produce free, charged analyte molecules that can be analyzed for their mass-to-charge ratio. Image taken from (El-Aneed *et al.*).

The analyzer "Time of Flight". As discussed above, different kinds of spectrometers differing by their ion sources but also by their analyzers exist and can be used to detect and identify the metabolites. The main analyzer types are the quadrupoles, the linear ion traps, the orbitraps, the time-of-flights or again the Fourier-Transform Ion Cyclotron Resonance (FT-ICR). In the case of the TIMSTOF-Pro-2 instrument, the analyzer is a time-of-flight (TOF). In this analyzer, ions formed in the source are accelerated with a constant voltage to provide to the ions a potential energy proportional to their charge and the acceleration voltage used (Equation 1). As the ions do not have all the same mass m, they will not have the same acceleration when subjected to this electric field (Equation 2). Finally, as ions reaches the end of the acceleration zone, the potential energy is fully converted into kinetic energy, the two equations can be equalized (Equation 3) and give birth to the main equation of TOF

analyzer, connecting the m/z ratio and the time of flight (Equation 4). This time is the time the ions take to travel the free-field tube of the TOF which has a known length (Boesl, 2017).

(1) $E_{pot} = q\ V$

(2) $a = \frac{q\ V}{m}$

(3) $E_{kin} = x_A\ q\ E_A = ½\ m\ v^2$

(4) $T = \frac{x}{v} = x\sqrt{\frac{m}{2\ qV}} = x\sqrt{\frac{m}{z} * \frac{1}{2\ eV}}$ with $v = \sqrt{\frac{2Ekin}{m}}$ and $q = z\ e$

Equation 1 to 4 with E_{pot} the potential energy of the ion, E_{kin} the kinetic energy, q the electric charge, V the acceleration voltage, m the mass of the ion, v the speed of the ion, x the distance traveled by the ion, z the charge of the ion, e the charge of the electron and T the time it takes for the ion to travel along the drift tube.

Depending on the instrument, one or several reflectors are used to reflect ions before they reach the detector. A reflector is an electrostatic mirror composed of several lens plugs at increasing repulsive potentials. A population of ions sharing the same m/z will inevitably flight to different (but close) velocities and be detected at close masses, instead of identical ones. This is due to fluctuations of the accelerating potentials that may occur within the source and are reflected as kinetic energy distributions. Using reflectors brings two advantages: this allows to construct a more compact instrument by reducing the height or length of the spectrometer (by reducing the length of the tube of flight), to improve the spectral resolution by increasing the length of the ion path and by correcting the fluctuation of kinetic energy provided to the ions. Indeed, in a population of ions sharing the same m/z, populations with higher velocities will penetrate deeper into the reflector and will travel a longer path than the slowest ones. Reaching the detector, the ion beam will be refocused and detected at (+/-) the same time. The improved resolution comes not only with the distance travelled by the ions, because the longer they travel the more they are separated, and the better the resolution of the instrument (Hosseini *et al.* 2017; Short *et al.* 1994), but also with a better focus of the ion beam (Figure 4).

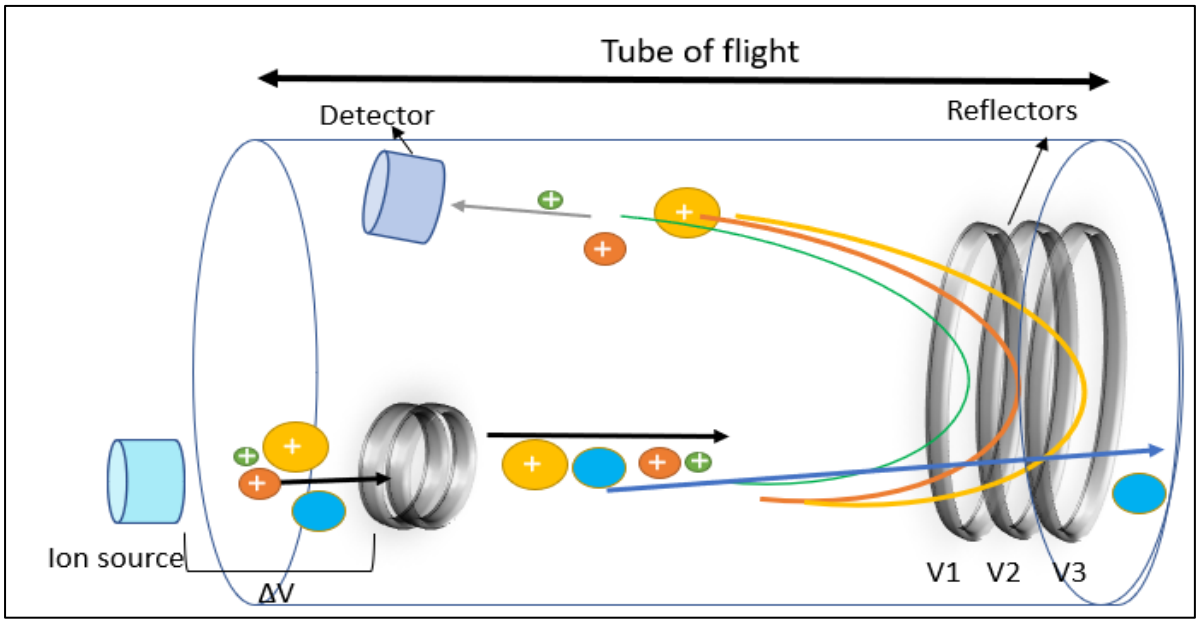

Figure 4. Schematic representation of the components of a TOF instrument with one reflector. The molecules are represented with circles (the ions are the molecules with a + in the circle). The arrows represent the trajectory of these molecules. For the reflectors, there is a ramp of potential so V1<V2<V3. Image made by Q. Bastiaens.

In the case of the TIMSTOF-Pro-2 spectrometer, ions formed by electrospray then accelerated, can be further separated by ion mobility, following the concept of trapped ion mobility spectrometry (TIMS, (Meier *et al.*, 2015, 2018, 2021; Ridgeway *et al.*, 2018)). As shown in Figure 5, the TIMS can be used to separate ions in the gas-phase depending on their collisional cross section, which is the probability of a collision taking place between the ion and a gas molecule. In the TIMS, the ionized molecules enter a cell and are propelled along the cell by a buffer gas flow. Along the cell are plates that exert an electric field gradient (voltage ramp) in the opposite direction to the gas flow. The ions are propelled by the gas but slowed by the electric field that is gradually increasing. At some point, the gas flow and the electric field apply equal and opposite force on one packet of ions, and they are trapped there. Since the force given by the gas depends on the ions' mobility (and their collisional cross section) and the force given by the electric field depends on their charge, the molecules are separated from one another along the cell and are trapped at a specific location. After this accumulation step, the voltage ramp's ending gradually decreases to transfer ions to the analyzer by small packets (D'Atri *et al.*, 2018; Heiles *et al.*, 2021; Meier *et al.*, 2015, 2018, 2021; Ridgeway *et al.*, 2018). Once the analytes are ionized and separated by the TIMS, the quadrupole can be used to select ions of a certain range in m/z. It filters the ions by creating an oscillating electromagnetic field between four metal rods (Chernushevich *et al.*, 2001). If the ion has the right m/z, in the range that was selected, its trajectory will be stable along the quadrupole's length, and it will progress further in the spectrometer, to the TOF and the detector. If the ion is out of range, its trajectory throws it out of the quadrupole, and it does not reach the next part of the instrument.

The TIMSTOF-Pro-2 is also able to perform tandem mass spectrometry (MS/MS) which allows for an even better identification of molecules. Activation can be performed through isolation of parent ions using a quadrupole in Data-Dependent Acquisition (DDA) or by using m/z and mobility windows in Data-Independent Acquisition (DIA). DIA has the advantage of fragmenting all the ions of the same packet coming from the TIMS. This reduces the time of analysis but has a huge drawback: it produces a large quantity of data that is hard to treat and requires a lot of computational power. To avoid this limitation, an evolution of the spectrometer has been set up. The TIMSTOF-Pro-2 possesses a parallel accumulation-serial fragmentation device (PASEF), that can be used to further separate the packet of ions. This technique is software based and uses a specific method of sampling to link ion mobility with the mass measured in TOF. This reduces the complexity of the DIA data because the software can directly link fragments to their own precursors (instead of having to determine the precursor for each fragment) (D'Atri *et al.*, 2018; Heiles, 2021; Meier *et al.*, 2015, 2018, 2021; Ridgeway *et al.*, 2018). The main use of this instrument will be to separate metabolites to identify them. The dual separation LC then TIMS greatly helps with the simplification of the analysis of the expected complex mixtures of compounds. The TOF analyzer will provide, in a second time, enough resolution to get a precise m/z for the ions. The TIMS separation operates one thousand times slower than the TOF which allows for the measurement of each packet individually. (Ridgeway *et al.*, 2018).

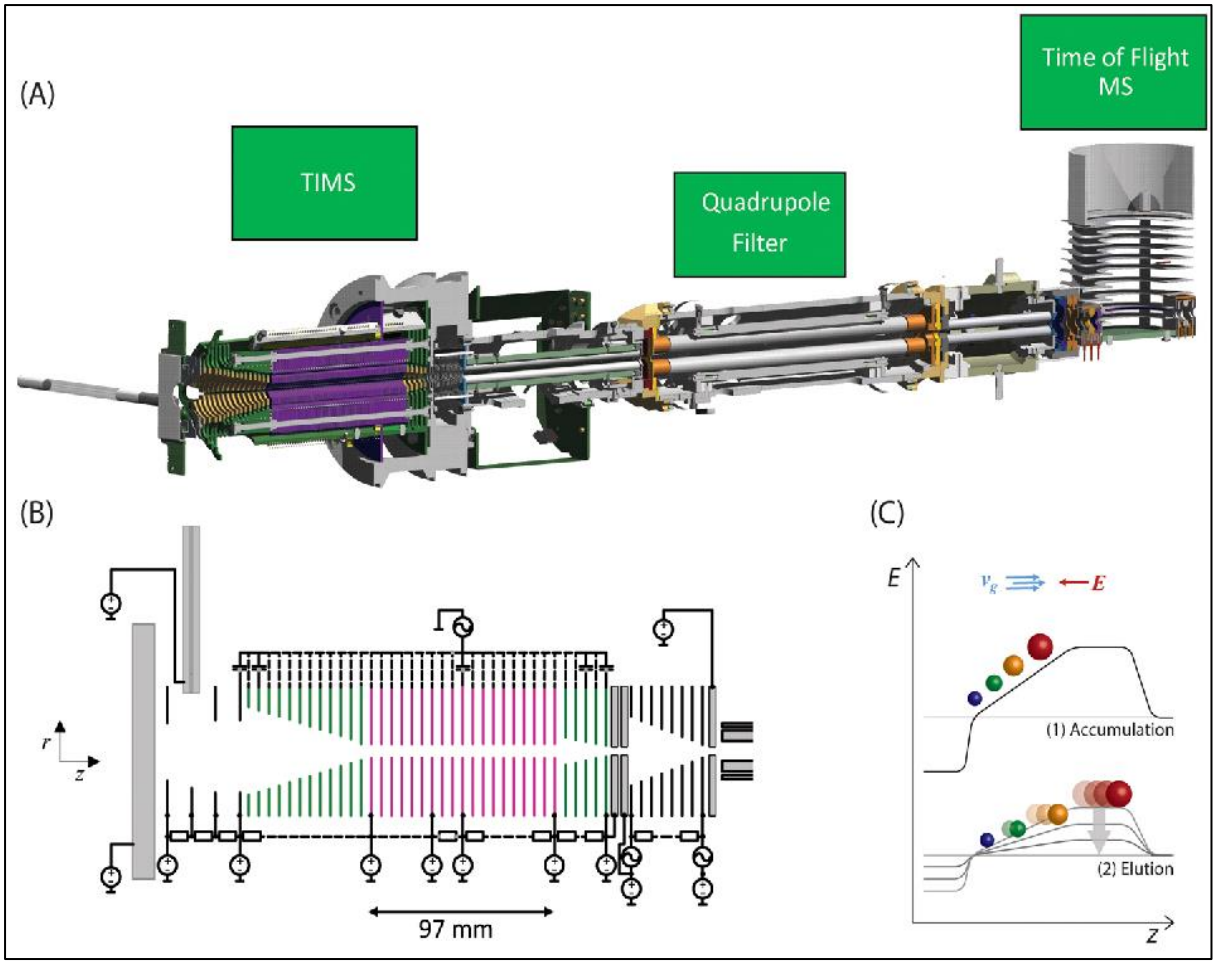

Figure 5. Trapped ion mobility spectrometry coupled to a QTOF mass spectrometer. (A) Instrument schematic of the prototype TIMS-QTOF instrument used in this study. (B) Detailed schematic of the TIMS tunnel (purple), enclosed by the entrance and exit funnels (green). (C) General mode of TIMS operation, including ion accumulation (1) and serial elution (2) of ion mobility separated ions from the TIMS device by decreasing the electrical field. The directed forces of the gas flow and electrical field are indicated by $_{v}g$ and E. Image taken from Meier *et al.*, 2015

D. Mass Spectrometry imaging, the key for unlocking spatial metabolomics.

Mass Spectrometry Imaging (MSI). MSI is performed by linking a mass spectrum to a discrete coordinate (x, y) of a sample data to obtain an image composed of hundreds or thousands of mass spectra. The images can be acquired using many different ionization techniques. One can cite Matrix Assisted Laser Desorption/Ionization (MALDI) (El-Aneed *et al.*, 2009; Mainini *et al.*, 2015), Secondary Ion/Neutral Mass Spectrometry (SIMS/SNMS) (McDonnell *et al.*, 2006), Desorption ElectroSpray Ionization (DESI) (He *et al.*, 2022; Karas *et al.*, 1985a; Parrot *et al.*, 2018), Laser Ablation Inductively Coupled Plasma Mass Spectrometry (LA-ICP-MS) (Becker & Jakubowski, 2009; Plsonero & Günther, 2008) and the Surface Assisted Laser Desorption/Ionization (SALDI) (Müller *et al.*, 2022) are the sources of interest to perform MSI. The main technique that will be used for this master thesis is MALDI, detailed in the section below, which will be performed using a Fourier-Transform Ion-Cyclotron Resonance mass spectrometer (FT-ICR MS).

Matrix-Assisted Laser Desorption/Ionization (MALDI). MALDI is a technique of desorption/ionization based on the utilization of a matrix to assist the ionization process and protect the analytes from

degradation. The matrix is usually a small organic aromatic compound that has the ability to co-crystallize with the molecule of analytes. During the irradiation of the crystals with a laser (UV range of wavelengths), the matrix will absorb the energy of the laser which causes a fast rise in the temperature of the crystals. This leads to the desorption of the matrix and the analytes, in a dense zone called the MALDI plume, where reactions between neutral and ions occur and may lead to the ionization of the analytes (Figure 6).

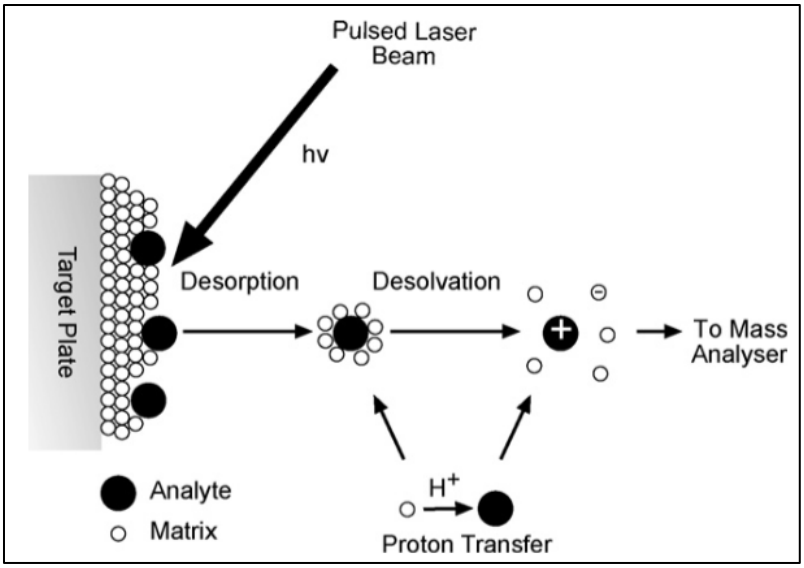

Figure 6. Scheme of the ionization of analytes using MALDI methods. The co-crystal of matrix and sample is targeted by a laser causing a desorption process followed by desolvation and then introduction into the mass analyzer. Image taken from (Kicman *et al.*, 2007)

This complex process is not entirely understood (Knochenmuss *et al.*, 2000; Knochenmuss *et al.*, 2023), however there are two different models that try to explain the process of ionization: the lucky survivor model and the gas-phase model (Jaskolla *et al.*, 2011). In the lucky survivor model, the matrix forms crystals with charged analytes (charge possessed in solution) and their counterion. When the laser irradiates the crystal, the matrix and the analytes are desorbed, leading to the formation of small clusters of ionized matrix molecules, charged analytes and their counterions. From there, two different phenomena can happen, either the cluster has a neutral net charge (and nothing happens) or since the crystal formation can separate ions, the cluster has a net charge. In the case where there is a lack of counterions for the analytes and the matrix, analytes can get protonated, and form singly charged analytes. These ions are ordinarily called “lucky survivors” (Jaskolla *et al.*, 2011; Karas *et al.*, 2000). In the gas phase model, analytes are neutral when they form the crystal with the matrix (either naturally or by recombination with their counterion). The ionization takes place, as the name suggests, in the gas phase when the neutral analytes collide with protonated or deprotonated matrix molecules. This collision induces proton transfer reactions. Depending on the case, this transfer occurs from the matrix to the analyte which is then protonated or from the analyte to the matrix which results in deprotonation of the analytes (Jaskolla *et al.*, 2011). Both models result in a soft ionization since the analyte never encounters an energetic source directly. Hillenkamp and his team were the first ones to use laser desorption/ionization (LDI) in 1985 on amino acids and dipeptides, because of their difference in absorbance of UV light. They determined that the wavelength of the laser and a matrix that can easily absorb UV light are key factors to obtain soft ionization of an analyte in LDI (Karas *et al.*, 1985a). They followed in 1987 with the first MALDI study ever (Karas *et al.*, 1987). This was later used to analyze high-molecular weight molecules (proteins and polymers up to 100,000 m/z) (Tanaka *et al.*,

1988) which resulted in Tanaka getting one third of a Nobel prize in 2002 along with John B. Fenn (for the discovery of ESI) and Kurt Wüthrich (NMR spectroscopy).
The nature of the matrix also has an influence on the desorption of molecules, their ionization and then their detection. For instance, the matrix background, made of ions and cluster of matrix molecules, is made of intense peaks that can influence the minimum m/z ratio at which analytes can be observed without the matrix interfering with the analysis. The detection of some families of molecules, like phospholipids, can, in some cases, only be done with certain matrix like α-cyano-4-hydroxycinnamic acid (HCCA) or 2,5 dihydroxybenzoic acid (DHB) because there tends to be ion suppressions effect which affect the detectability of these analytes (Leopold *et al.*, 2018; Perry *et al.*, 2020).

Principle of Mass Spectrometry Imaging. One of the downsides of MS for metabolomics is that the solutions studied must be representative of the sample and no spatial information can be recovered from MS data. But in this case, MALDI can be used to perform mass spectrometry imaging (MSI) of a sample to regain that lost piece of information. The sample is prepared by cutting the sample in slices, transferring the slices to a conductive slide, and covering the sample with a matrix (Figure 7). However, instead of obtaining data randomly on a spot, in imaging, the laser scans the entire area of the sample surface methodically. The spot made by each laser shot gives out an MS spectrum for a zone which is called pixel. A series of pixels is obtained, and since we know the laser's position for each shot, an image of the sample for a particular m/z can be reconstructed. Each pixel is linked to a mass spectrum containing the information about the metabolites/compound detected at this discrete position.

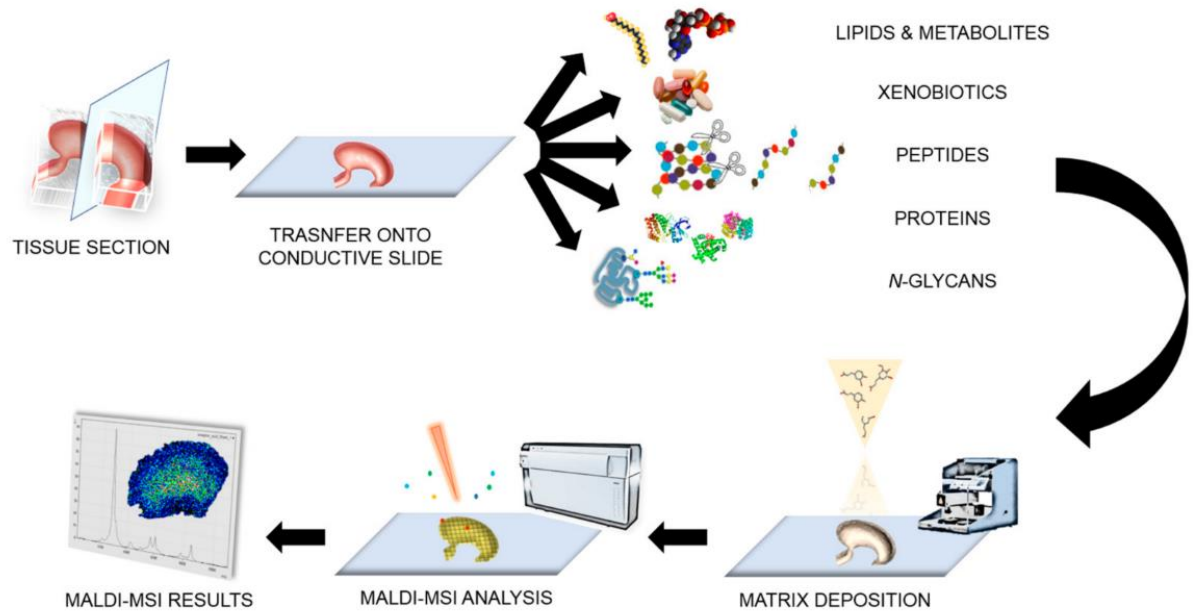

Figure 7. Illustration of the workflow for the matrix-assisted laser desorption/ionization-mass spectrometry imaging (MALDI-MSI) analysis. Image from (Smith *et al.*, 2017)

This process has been used to obtain images and spectra for tissue slices since 1997 (Caprioli *et al.*, 1997). Since the sample preparation plays a key role to obtain useful information, Schwartz *et al.* developed a method to limit spatial migration and sample damaging by washing the slices in 70% ethanol and using 50% ethanol or acetonitrile with 0.1% Trifluoroacetic acid (TFA) as a solvent for the matrix (Schwartz *et al.*, 2003). They also realized that sinapinic acid was one of the best matrices since

it brought a good compromise between crystal size and signal quality, leading to an increase of spatial resolution. The washing part was later improved by Lemaire *et al.*, who found out that chloroform, acetone, hexane, toluene, or xylene were ideal solvents to wash samples to get rid of unwanted molecules such as lipids (in the case of proteomics) without removing peptides and proteins (in contrast ethanol, chloroform/xylene, which are the usual solvents, remove part of the metabolites, peptides and/or proteins) (Lemaire *et al.*, 2006). Tests were also performed to determine which matrix is the most adapted for the analysis of families of molecules such as proteins and peptides. It seems that ionic liquid matrices such as α-cyano-4-hydroxycinnamic acid (CHCA) coupled with N,N-dimethylaniline (DANI) or aniline (ANI) improve the signal and allow negative mode ionization (Lemaire *et al.*, 2006). Unfortunately, DANI and ANI are very toxic and can have a long-term effect on human health. There is no real "best matrix" for MALDI and the matrix must be chosen through trial and error according to the sample studied (Liu *et al.*, 2022). Lastly, the data processing was optimized by Norris *et al.*, they used softwares that removed the baseline, normalized the data, and made a spectral recalibration/ realignment to improve the signal/noise ratio and to obtain more reproducible results. These improvements are not specific for a sample but allow for easier detection and profiling of peptides and proteins. But also, they bring a gain in contrast and compensate for part of the imperfections of the matrix such as the size of the crystals, surface defects and differences in quantity of matrix throughout the surface. This method can be applied as a base for the development of a specific study for a sample, regardless of the method (proteomics, metabolomics, lipidomics,…) (Norris *et al.*, 2007).

In addition to MALDI, other noteworthy methods include SIMS/SNMS, DESI, LA-ICP-MS and SALDI. SIMS/SNMS uses a highly energetic ion beam, as primary species, which is pulsated on a solid sample. The ion beam can be composed of noble gases, oxygen species, small molecules, or heavy atoms such as ^{133}Cs. The collision between the ions and the sample causes sputtering of secondary species from the sample which are then recovered in the mass spectrometer for analysis. Depending on if the molecules desorbed are either ions or neutrals, separates SIMS and SNMS. This technique will fragment the ions because of the energy possessed by the ion beam of the source which can be useful for the analysis of some molecules but is also a disadvantage if the sample has to stay in its natural state. However, it can be used to probe a surface because of its spatial resolution (< 100 nm) (McDonnell *et al.*, 2006). DESI uses an electrospray source to spray a solvent on a solid sample, this desorbs some molecules from the sample and causes the ionization of a fraction of them. The desorbed ions are then sent to the mass spectrometer. The main advantage is its ability to obtain quick results with little sample preparation compared to MALDI. Unfortunately, the spatial resolution and the sensitivity of this method are poorer than other techniques (He *et al.*, 2022; Karas *et al.*, 1985b; Parrot *et al.*, 2018). LA-ICP-MS is a laser ablation technique that works by irradiating a sample by a laser beam, without the addition of matrix. The energy transferred from the laser to the sample sublimates the analytes and ionizes some of them. The evaporated molecules are then sent to a plasma torch of an inductively coupled plasma mass spectrometer using a vector gas (usually helium). The analytes are atomized by the plasma torch and the atoms composing these analytes are analyzed to obtain the atomic composition of the sample (Plsonero *et al.*, 2008). This technique is highly destructive and no structural information can be obtained which limits its use in organic chemistry. But for geological analysis of rock fragments, in inorganic chemistry or for archaeology for example, this technique is demonstrated powerful to obtain information about the composition of unknown samples or the impurities present in synthetic materials. SALDI is in a first approach close to MALDI. The main difference is that it uses the modified/ structured surface of the plate (where the sample is deposited), to absorb the energy of the laser instead of a matrix. After the pulse, the energy of the laser is transferred to the surface then from the surface to the sample. After the transfer of energy,

part of the sample is desorbed from the surface and a portion of the desorbed molecules are ionized. The ions are then sent to a detection cell like in MALDI (Müller *et al.*, 2022). The main advantages of this technique are that there is almost no sample preparation needed before an analysis. The absence of the matrix molecules allows for a better lateral resolution than MALDI because the size of the crystal normally limits the maximum resolution achievable. The last major advantage is that small m/z (<900Da) can be measured without the interference of matrix molecule signals, usually very intense in MALDI. The main downside is the unknown mechanism for this technique which makes the first experiments' results unpredictable. There is also a limit in the mass range, high molecular mass molecules tend to not get desorbed or not ionized if desorbed from the surface. Most of these techniques are complementary and are rarely competitive with one another due to their limitations, use and area of applications.

In this master thesis, MALDI-MSI only will be considered. This ionization source can be coupled to various mass spectrometers, equipped with different analyzers. The MS-Lab of ULiège has the chance to possess a FT-ICR, one of the best spectrometers currently marketed.

Fourier-Transform Ion-Cyclotron Resonance Mass Spectrometry (FT-ICR MS). The FT-ICR instrument available in the laboratory is a 9.4 T SolariX® from Bruker (Germany) (Figure 8) mounted with a ParaCell® (Boldin & Nikolaev, 2011; Nikolaev *et al.*, 2011) and a dual source ESI/MALDI. Concerning the MALDI facility, the spectrometer is composed of a sample holder, a laser, an ion funnel, a quadrupole to select ions, a collision cell that can be deactivated, an octupole to guide ions and the detector. Once the analytes are ionized, here by MALDI, the quadrupole is used to let all the ion of a certain mass range have a stable trajectory or to select a particular ion of a certain m/z to be fragmented in the collision cell. The octupole works similarly to the quadrupole but is set so that every ion has a stable trajectory along its length. After passing through them, the analytes arrive at the FT-ICR detection cell.

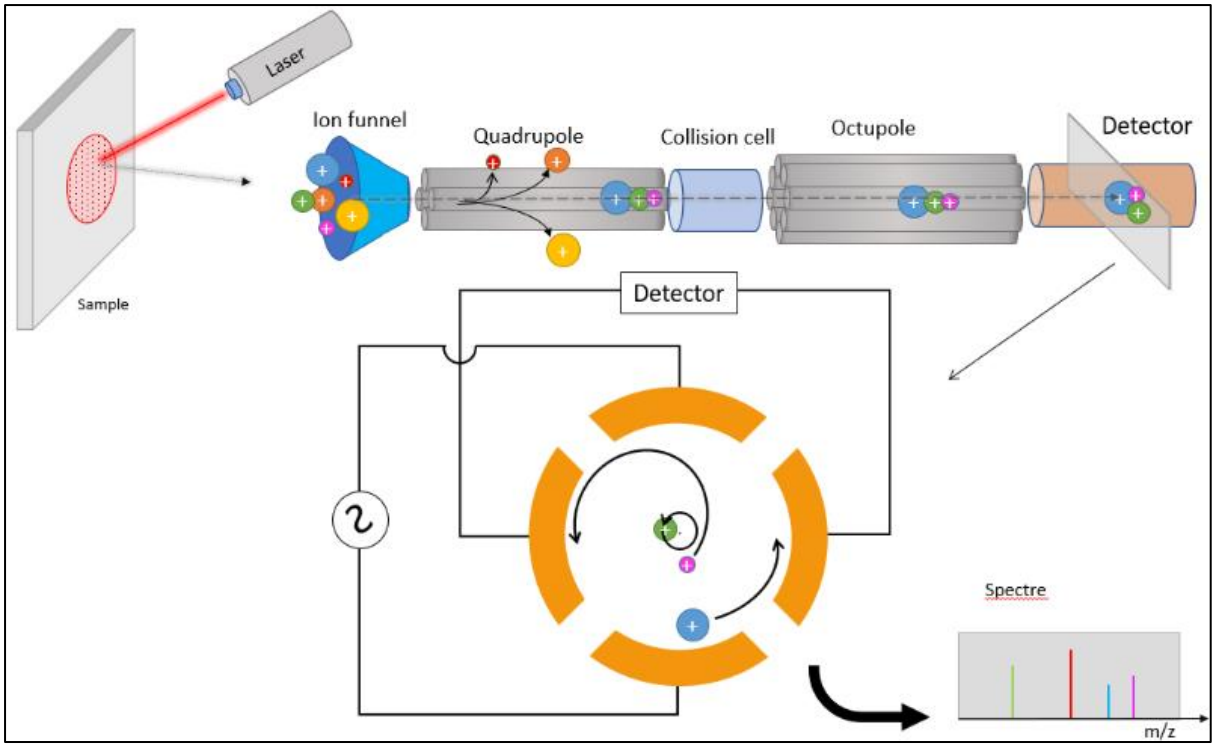

Figure 8. Schematic representation of the components of a MALDI FT-ICR instrument. The molecules are represented with circles (the ions are the molecules with a + in the circle). The arrows represent the trajectory of these molecules. Image made by Q. Bastiaens

FT-ICR analyzers have been developed by Alan Marshall and have proven to be a useful technique for metabolomics study of organisms (Brown *et al.*, 2005; M. Wang & Marshall, 1988). In FT-ICR-MS, the detection cell is a Penning trap composed of six plates: two trapping plates, two excitation plates and two detection plates. The trapping plates exert an electric force to change the trajectory of the ions that are in a strong magnetic field coming from a superconducting magnet. This results in the ions oscillating in the cell following an epitrochoid trajectory. The ions, once trapped, are accelerated by an oscillating field perpendicular to the magnetic field coming from the excitation plates to be promoted to a larger cyclotronic radius. Once a charged particle passes close to the detection plates, a current is generated in the plates (named image current). Since the ions are rotating at a certain frequency, the image current appears as a periodic signal. The frequency of this signal is dependent on the mass-over-charge value of the charged particle, thus allowing a separation of the ions (H. Y. Wang *et al.*, 2011). The oscillating field sweeps different values to excite different range of m/z of ions. The frequency of the ions can be given by:

$$f = \frac{qB}{2\pi m}$$

with f = cyclotron frequency (H)z,q=ion charge (C), B=magnetic field strength (T) and m = ion mass (amu)

The longer the analytes are trapped inside the detection chamber, the more precise the measure of their m/z can be. The frequency of oscillation is inversely proportional to the m/z of the ion, therefore by using a mathematical tool called the Fourier Transform (FT) the measured signal (sum of the frequencies of all the detected ions) can be deconvoluted and transformed into the mass spectra of these ions. The stronger the magnetic field the higher the resolution, with a powerful enough electromagnet and with enough time to analyze this technique can yield results with sub part per million (ppm) precision (Misra Gauri *et al.*, 2019; Ahamad *et al.*, 2022).

This instrument will be used in imaging to locate the metabolites previously identified with the TIMSTOF-Pro-2. The main goal will be to find in which organ(s) each metabolite or group of metabolites are commonly found. This will provide spatial information in addition to the identification as well as a potential role to the metabolite or group of metabolites of *Steatoda nobilis*.

At the time of this study, no metabolomic research were on whole spiders' bodies, whatever by LC-MS/MS or by MSI, although metabolomic studies were performed on the venom of 70 species of spiders (Klupczynska *et al.*, 2018), on the lipids of yellow scorpions' venom (Acunha *et al.*, 2023) as well as the lipids of the venom of *Hottentotta saylcyi* (scorpion) (Ghezellou *et al.*, 2022). The metabolites of some insects were also studied (20 species of mosquitoes, the common fruit fly (*Drosophila melanogaster*), the Rove beetle (*Paederus riparius*), the desert locus (*Schistocerca gregaria*), the turnip sawfly (*Athalia rosae*), the duff-tailed bumblebee (*Bombus terrestris*) as well as three butterflies: the monarch (*Danaus plexippus*), the common crow butterfly (*Euploea core*) and the cotton bollworm (*Helicoverpa armigera*), (Dreisbach *et al.*, 2023; Horvath *et al.*, 2021; Yang *et al.*, 2020). Some of these insects were additionally studied using MSI, but due to the complexity of the data most of the studies limited themselves to specific part of the sample, or to specific molecules or families of molecules (targeted approach) instead of studying the entire metabolome (untargeted approach).
These approaches focus either on specific metabolites or target a specific part of a target. The main goal of this thesis is to perform a metabolomic study on whole-body spiders with an untargeted approach.

II. Investigating *Steatoda nobilis* metabolome by MS- based approaches: Goal and Objectives

The primary objective of this master's thesis is to develop a comprehensive protocol for conducting metabolomic analyses on entire arthropod organisms, with a specific focus on the intermediary subject of *Steatoda nobilis*. The investigation also seeks to determine the reliability and suitability of employing LC-MS/MS, coupled with mass spectrometry imaging, in unraveling the complexities of arthropod metabolomics. This multifaceted exploration is expected to significantly contribute to the understanding of arthropod biology and advance the field of metabolomic analysis in these organisms. This master thesis will be consequently organized into two main parts:

(i) **Liquid chromatography and mass spectrometry: the duo of choice for metabolome investigations.** Using a coupling between liquid chromatography to separate the metabolites and a mass spectrometer (TIMS-TOF) to identify the molecules by their mass and their fragmentation spectra. Indeed, no study describing in detail the content of arachnid's metabolome has been published so far. Our study will not only constitute the first one in the field but will also improve the global knowledge about *Steatoda nobilis*, which needs to be controlled in the UK.

(ii) **Mass Spectrometry imaging, the key for unlocking spatial metabolomics**. Developing Mass Spectrometry Imaging (MSI) on the full-spider body to localize the metabolites directly within the spider's body, and more precisely in its organs and tissues. As we will demonstrate in the next sections, this approach is particularly challenging not only in terms of data analysis, but also in terms of sample preparation.

III. Materials and methods

A. Materials

All *Steatoda nobilis* spiders were collected in their natural habitat in Galway by Dr. John Dunbar. Twenty-one spiders were collected by night, walking and capturing them on their web. From these, there were ten females, all adult, and eleven males, six of which were pre-adults and five were adults. The adults were first kept at 8° C to slow their metabolism so as not to provoke any changes in the spiders due to the change in living conditions. The rest were regularly hydrated and fed with *Acheta domestica* so the pre-adults would mature.
The MALDI matrices, α-cyano-4-hydroxycinnamic acid (HCCA) and 2,5 dihydrobenzoic acid, as well as the other reagents fluoroacetic acid, and trifluoroacetic acid (TFA) were purchased from Sigma-Aldrich (Belgium). The methanol and the acetonitrile were UHPLC–MS grade from Biosolve® (Belgium) and the water used was miliQ water produced in the lab (Merck, Germany).

B. Analytical systems

The HPLC used was an Acquity UPLC M-Class (Waters, Milford, MA, USA). The LC is equipped with two columns: first an analytical column which was a HSS T3 C18 1.8 µm (75 µm × 250 mm) and second a trap column which was a Symmetry C18 five µm (180 µm × 20 mm) (Waters, Corp., Milford, MA, USA). The samples were loaded at ten µL/min on the trap column in H_2O/ACN/Formic acid (99/1/0,1, v/v) for three min and were eluted using a gradient going from the original 99 % water, 1 % acetonitrile 0,1 % formic acid to 1 % water, 99 % acetonitrile 0,1 % formic acid at a flow rate of 0.6 mL/min.
The mass spectrometer used for the LC-MS/MS was the TIMS-TOF pro 2 (Bruker Daltonics, U.S.A.) equipped with en ESI source. The samples passed through the TIMS with a gas pressure of 2.6 mbar with N_2 as the drift gas and a drying temperature of 180 °C. After that, the samples were ionized by sing a capillary voltage of 4.7 kV and then sent to the mass spectrometer where the scan range was set to 50 m/z – 1600 m/z.
The mass spectrometer used for the imaging was the 9.4T SolariX® (Bruker Daltonics, Germany). The calibration was performed with red phosphorous before each imaging run from 200 m/z to 1600 m/z in order to reach an accuracy below 1ppm. The data was acquired with a file size of 4M (resolution of 1,000,000 at 400 m/z). For the acquisition, the software used was the FlexImaging V.5 (Bruker Daltonics, Bremen, Germany), the pixel step size for the surface raster was set to 50 µm. The laser beam focus was set to “minimum” while the power was set to 25 %, with 300 laser shots per spot at a frequency of 2000 Hz.
Other instruments used include the SunCollect® Micro-Fraction Collector/MALDI Spotter (SunChrom®) to spray the MALDI matrices and the CryoStar NX70® (ThermoFisher® Scientific, Massachusetts) to cut the slices, both instruments are described below.

C. LC-MS/MS investigation of *Steatoda nobilis* metabolome

Extraction of the metabolites. For doing metabolomics by LC-MS/MS, the metabolites must be extracted from the tissues and purified to get a homogenous liquid phase, ready to be injected in the system. For initiating the extraction step, biologic tissues are usually transformed into a powder to improve the quality of the extraction. To achieve this, entire spiders are asleep using a CO_2 chamber, then flash-frozen in a bath of iso-pentane, cooled by liquid nitrogen. The spiders are then crushed into a fine powder. However, even if a classical spider body is soft at living temperature, its abdomen cuticle becomes incredibly resistant once frozen which makes the manual crushing very hard. The spiders were anyway powdered carefully using a pestle and a mortar, previously cooled at 77 K (≈ -196° C) as well. The powder was collected in classical plastic tubes (Eppendorf®) while any remaining traces adhering to the mortar were retrieved using 800 µL of a solution of methanol and water (80/20, v/v).

The protocol of metabolite extraction from the powder was adapted from the recent literature. The powder, suspended into the 800 µL of MeOH/H_2O (80/20, v/v), underwent a 15 min sonication process using a Branson 1510 ultrasonic cleaner (Branson, USA) then centrifuged at 7200 G for 2 min in an Eppendorf® 5415 R centrifuge (Eppendorf®, Belgium). The supernatant was collected and recovered in an Eppendorf® plastic tube and 500 µL of a fresh solution of MeOH/H_2O (80/20, v/v) was added to the remaining pellet. This operation was repeated 3 times for each sample to maximize the extraction (Gutiérrez *et al.*, 2022; Horvath *et al.*, 2021; Karger *et al.*, 2012; Saber *et al.*, 2018; Scaraffia *et al.*, 2006; Vial *et al.*, 2020; Zangrando *et al.*, 2020)..

Because of the nature of the samples that may still contain some particles of suspended crashed tissues, it was decided to insert an additional step of purification to prevent any risk of clogging of the LC system. Thus, after the centrifugation, the supernatants were filtered using Amicon® Ultra-4 filters 10KDa, 4ml (Sigma-Aldrich, Belgium) by centrifugating it at 7200 RPM in an Eppendorf® 5430 R centrifuge (Eppendorf®, Belgium), for 240 minutes. After being filtered, the filtrates were lyophilized by using a SpeedVac (ThermoFisher®, Germany).
To prepare the samples for the injection in LC-MS/MS, they were diluted in two mL of H_2O/ACN (99/1, v/v). As it was impossible to evaluate the concentration of extracted metabolites in our samples and to avoid any overload of the LC column, additional dilutions of 1:1000, 1:100 and 1:10 were prepared. The most diluted one was first injected and the results are described below.

D. MALDI-Mass Spectrometry Imaging tissue sample preparation for spatial metabolomiocs of *Steatoda nobilis*

Making a sample preparation destinated to mass spectrometry imaging is never straightforward and needs to take care of each step to ensure the best result possible. When the sample is a entire spider, composed of inhomogeneous smooth and hard tissues, it is even worse. The main steps followed to reach the imaging of the spider are schematized Figure 9.

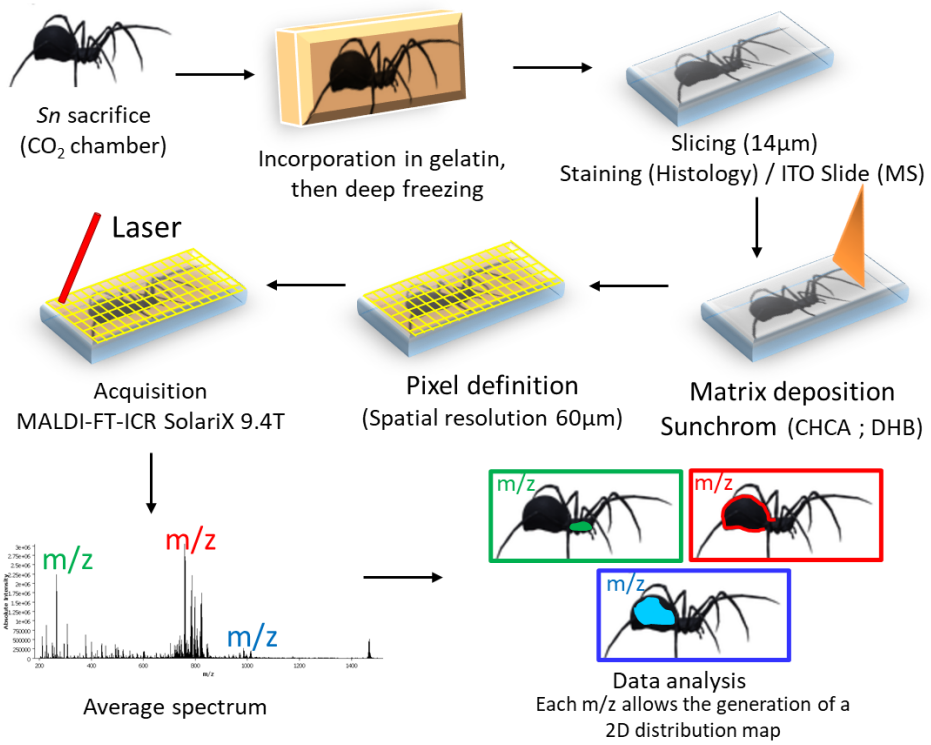

Figure 9. Illustration of the protocol for the preparation of Steatoda nobilis for MALDI MSI.

Spider preparation. Classical tissue preparation is not adapted to spiders as they are not composed of large homogeneous tissues and their various organs must be preserved during the slicing step. The best compromise found was to embed the animals into frozen gelatin to maintain the organisms in good shapes. To do so, gelatin was poured in a mold and dissolved in water at 60 °C. Then, once the gelatin dissolved, the spiders were put to sleep using a CO_2 chamber, before being immersed in the gelatin. The samples were then deep frozen in pentane, cooled with liquid nitrogen. The block of gelatin containing the spiders were unmolded and stored at -80 °C.

Tissue sectioning. Once the spiders incorporated into the frozen gelatin, the sectioning was performed on a cryotome CryoStar NX70® (ThermoFisher® Scientific, Massachusetts) set at −20 °C. For the sectioning, SEC35e low-profile razor blades (ThermoFisher® Scientific, Massachusetts) were used at −18 °C. The whole-body sagittal slices of *Steatoda nobilis* were initially prepared at a thickness of 14 µm, but such thin sections tended to degrade in the MALDI source. Indeed, these slices were too thin to adhere enough to the MALDI plate and resist to the vacuum of the source. New sections were cut at thicknesses of 25 µm or even 30 µm in the case of the male spiders because males are smaller than females and possess a weaker resistance to the cutting process (*personal observations*). The sections were cut according to the sagittal plane, as much as possible in the middle of the spider (Figure 9) to try to observe a maximum of organs in the spiders.

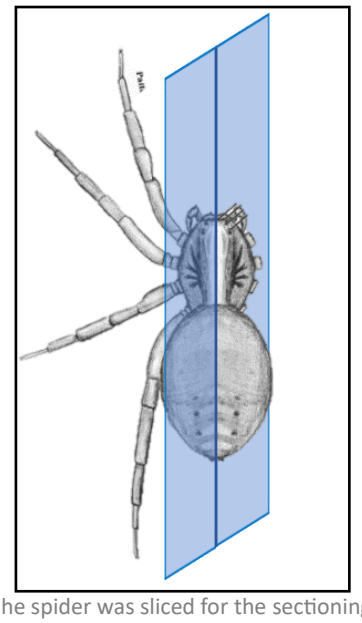

Figure 9. Schematic representation where the spider was sliced for the sectioning (half of the body in sagittal plane).

Slice histological coloration. To get a reference for our MS images, a serial slice was colored with haematoxylin and eosin (H&E) (Figure 10). Haematoxylin is a compound which is used to see the stain the cell nucleus while eosin is used to stain the extracellular matrix. This allows for a contrast image with the different organs standing out from the main body. For the coloration process, the slices, after being mounted on glass slides, were dipped in a series of baths as follows. Initially, the slices were immersed successively for 4 seconds in 100 %, 90 %, and 70 % ethanol solutions, followed by a 4-second deionized water Subsequently, a 2-minute soak in a hematoxylin bath occurred, succeeded by a 2-second wash in a 0.1 % HCl bath and a 3-minute water rinse. They were then soaked for one min in an eosin bath followed by four seconds in a water bath then successively four seconds in a 70 %, 90 %, 100 % ethanol solution to rinse. Once ready, the slices are put under a microscope to obtain a high-resolution image.

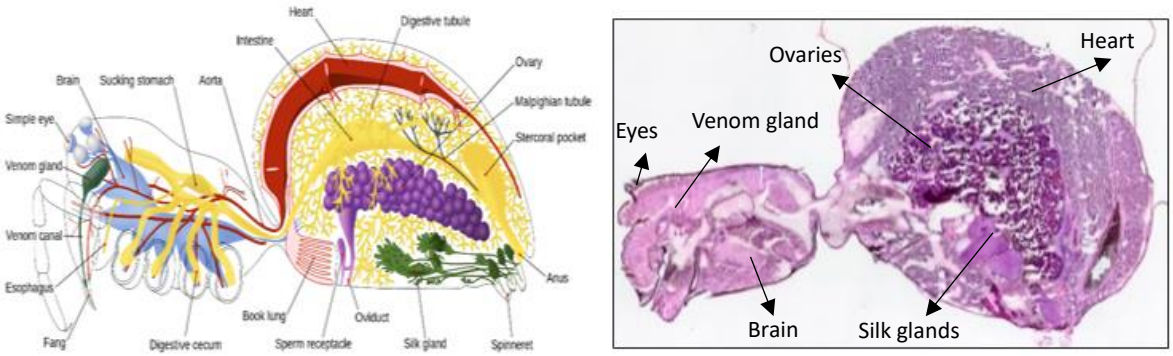

Figure 10. Results of the H&E staining. On the left side is an anatomic drawing of a spider [1], on the right is a female sample stained with H&E.

Cryosections meant for the MALDI analysis were thaw-mounted onto indium tin oxide (ITO)-coated conductive glass slides (Bruker® Daltonics, Bremen, Germany) which were then coated with a matrix for the MALDI processing.

[1] taken from http://blackwidowspiderresource.weebly.com/respiratory-system.html

Matrix coating. For MSI experiments, two different matrices were considered α-cyano-4-hydroxycinnamic acid (HCCA) and 2,5-dihydroxybenzoic acid (DHB). Both matrices were used in positive ion mode to generate ions such as $[M+H]^+$, $[M+Na]^+$, $[M+K]^+$ or $[M+NH_4]^+$. HCCA was chosen because of its capability to desorb and ionize low mass molecules (metabolites) while forming very low mass adducts (>150 m/z) that do not impede much for the analysis (Angerer *et al.*, 2022). DHB can desorb low mass molecules and larger one as well, but forms higher mass adducts (up to 300-400 m/z) thus low mass molecules cannot really be analyzed since the matrix covers the low range m/z (Mielczarek *et al.*, 2023). DHB was chosen because it might bring different information than the HCCA and may open the gate to the observation of higher mass compounds such as larger metabolites or peptides.

The matrices were sprayed onto the histological slices with a SunCollect® Micro-Fraction Collector/MALDI Spotter (SunChrom®), layer by layer, to reach a good coverage of the sample by the matrix, to get small crystals, while limiting the potential delocalization of the metabolites. The crystal shapes and the delocalization of the compounds must be carefully controlled to ensure a good spatial resolution on the image. HCCA and DHB depositions have already been partly optimized in the laboratory, but some tests were still carried out to further optimize the method, based on this article (Mielczarek *et al.*, 2023). HCCA was sprayed in 13 layers, whereas DHB needed 15 ones. The concentration of matrix for each layer is different, the first layer was sprayed with 10 µl/min, the second with 20 µl/min , the third with 30 µl/min, the fourth and fifth with 40 µl/min and then the rest are sprayed with 60 µl/min (summarized in table 1).

Table 1.Quantity of matrix for each layer.

Layer n°	Quantity sprayed (µl/min)
1	10
2	20
3	30
4-5	40
6-16	60

E. Bioinformatic treatment using softwares for Mass Spectrometry Imaging analysis.

Mass Spectrometry SCiLS® software. SCiLS® software is the dedicated tool provided by the spectrometer manufacturer (Bruker) to assess the quality of the results, to get an overview on the average mass spectrum and to generate images from a selected peak (m/z) or a range of m/z. For this master thesis, this software was used to export the data under a ".imzml" format, compatible with other dedicated softwares and to perform one analysis using the built-in tool "segmentation". This tool treats the data obtained during an imaging run and separates pixels based on the similarities between their spectra. If several pixels, close to one another, have some ions in common but that are not present in the rest of the image, then the software groups these pixels in a zone. This zone can then be broken down into successively smaller zones, until there are not enough ions in common between pixels for them to form a zone. However, it is important to note that the ions separated by the software are not mentioned in the final product of the segmentation. Only an image with all the different zones is obtained and the color code for each zone is random and imposed by SCiLS®

Mass Spectrometry Kendrick Filter software. To facilitate the analysis, we additionally used Kendrick Mass Defect (KMD) filter software. This home-made software (Dr Christopher Kune) is based on the exploitation of mass defects according to Kendrick's method (KMD). This approach is based on a two-dimensional projection of the atomic or molecular composition space, allowing the classification of the molecules according to their structural similarities which leads to a faster and easier identification of the families of homologous compounds. KMD analysis consists in a base transformation of the mass spectra to the Kendrick base. The mass spectra, a graphical representation in the form Intensity = f(m/z), is transformed into the form KMD = f(m/z). The principle of the Kendrick base is to horizontally align molecules who share the same elemental composition (= same KMD) and differ only by a number of defined building blocks, called base that is definite by the user. The classical base unit of mass is 1/12 of the mass of the ^{12}C (IUPAC), but in the Kendrick base, a new reference base unit is chosen. For metabolites and lipids, the chosen base is usually CH_2 as lipids differ among the same family according to their number of CH_2 and their number of unsaturation. In the case of CH_2, the new base unit of mass is 14.0000 instead of 14.0157 in the IUPAC scale. Using this new base, the masses of all the ions are recalculated and are displayed on the Kendrick spectra (Kendrick, 1963). The KM and KMD are calculated as follows:

- KM = $\frac{m}{z} * \frac{\text{KRnominal mass}}{\text{KRexact mass}} = \frac{m}{z} * \frac{14}{14{,}01565}$ KMD = KM (integer/round) – KM_{exact}

On the Kendrick plot (KMD=f(m/z)), molecules that only differ by their number of CH_2 (which is very common in metabolomics/lipidomics) share the same mass defect but have different masses (Figure 11). The consequence is that such molecules will be horizontally aligned on the Kendrick plot. If it the number of unsaturation varies, the masses of these molecules will vary by 2 Da (2 hydrogen atoms) and will appear aligned diagonally because the KMD difference will always be the same when the number of unsaturation vary, and the masses will vary by around 2 m/z.

These aligned molecules (horizontally and diagonally) are usually part of the same family and are easily separated from the rest of the spectra. The appeal of this method is that once one of these molecules has been identified, all the others can be found rapidly and straightforwardly. This simplifies the analysis by dividing the data into smaller groups that are easily identifiable while the ions that are not part of any family stand out from the rest and can be processed independently. This reduces the quantity of data anywhere from 30 to 80 % depending on the number of molecules that belong to the same family that were ionized and sent to the detector (McCann *et al.*, 2021).

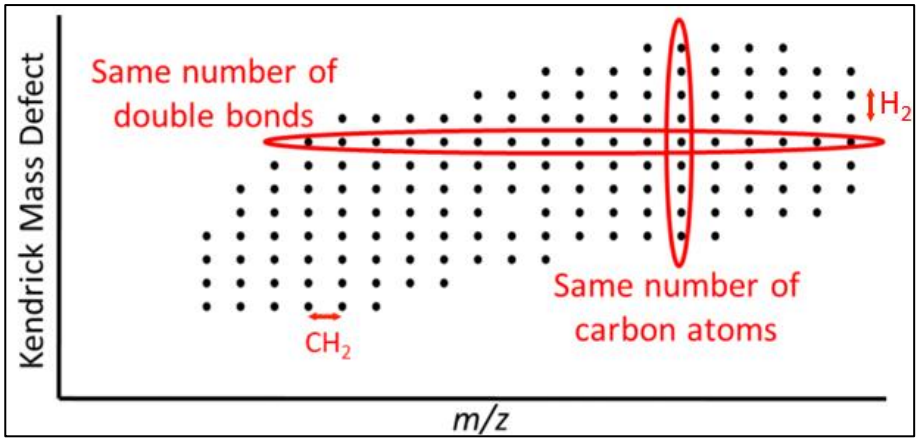

Figure 11. Illustration of a Kendrick plot. Each dot is a compound, the horizontal distance between two dots is linked to one CH2 unit and the vertical distance between two dots corresponds to two hydrogens. Image taken from Hustin *et al.*, 2022

Mass Spectrometry Metaspace® software. Metaspace® is a high-performance search engine, made for the identification of metabolites from mass spectrometry imaging data. Metaspace® yields a wealth of information, encompassing the potential raw formula of the detected ion based on the experimental m/z, the molecules that may correspond to this raw formula, the structural elucidation of these candidate molecules, the spatial localization within the image of the ion of interest, conceivable adducts associated with the identified molecules, and, significantly, additional ions exhibiting colocalization. In Metaspace®, users have the flexibility to select multiple databanks such as LipidMaps, SwissLipids or CoreMetabolome (main databanks used in this master thesis) to perform identification of a given sample.

IV. Results

I. LC-MS/MS analysis results

Extraction of the metabolites. Following the first protocol of metabolite extraction drove to disappointing results. Indeed, the chromatograms and mass spectra exhibited peculiar characteristics. Notably, a limited number of ions were detected, albeit in relatively high concentrations. The LC-MS/MS of the samples diluted at 1:1000 revealed four intense peaks, surpassing at least one hundred times the intensities of the other constituents (Figure 12, in red-orange).
On the mass spectra corresponding to this sample (Figure 13), the main detected peaks are separated from each other's by 74 Daltons. This indicates these signals belong to a contaminant that has a repeating unit of 74 Da and is probably a polymer. This repeating unit corresponds to dimethylsiloxane which might correspond to the coating of the tubes used to store the samples. Subsequent investigations unveiled these ions as contaminants originating from the plastic tubes (Eppendorf®) and the Amicon® filters. To determine the source of the contaminations, blank experiments involving the use of plastic tubes or Amicon® filters only were considered. When only plastic tubes are used, contaminants are detected in the three last peaks in the chromatogram's (Figure 12, in blue). On the other hand, tests employing Amicon® filters displayed an additional contribution in the first peak (Figure 12, in green), the global contamination patterns being close to the one observed for our biological sample (red), and identical to the blank submitted to both plastic tubes and Amicon filters (Figure 12, in purple). The first peak linked to Amicon® filters has a very low intensity compared to the one obtained for the biological sample. Corresponding mass spectra unequivocally identified this contaminant back to their source. The variation of intensity is probably linked to the time of filtration involved. Indeed, the biological sample was subjected to a filtration of around 4h, whereas the blank, less viscous and containing no large particles, has been filtered for 1h only, limiting the contamination. The second peak, stemming from both plastic tubes and Amicon® filters, suggested a potential similarity in the coating on the tubes. After checking the chromatogram, the mass spectra were also investigated, revealing that the ions present in the sample (Figure 13) were also present in the mass spectra of the 3 blank tests. The contamination hypothesis posits that during sample preparation, the MeOH/H_2O mixture employed for extraction inadvertently extracted the coating from the plastic tubes, likely damaging the Amicon® filters in the process. Consequently, the contaminants were substantially co-extracted with the remaining metabolites.

A significant challenge arose from the concentrated nature of these contaminants. Amplifying the sample concentration to increase the probability to observe metabolites risked causing a saturation of the column by the contaminants, and potentially obstructing and damaging the LC system. Moreover, the contaminants dominated a substantial portion of the chromatogram and exhibited such intensity in the MS spectra (Figure 13) that other components might be hidden even with increased concentration (ion suppression effect). The resolution to this predicament involved eliminating the additional security step of filtering and adopting glass tubes in lieu of plastic tubes.

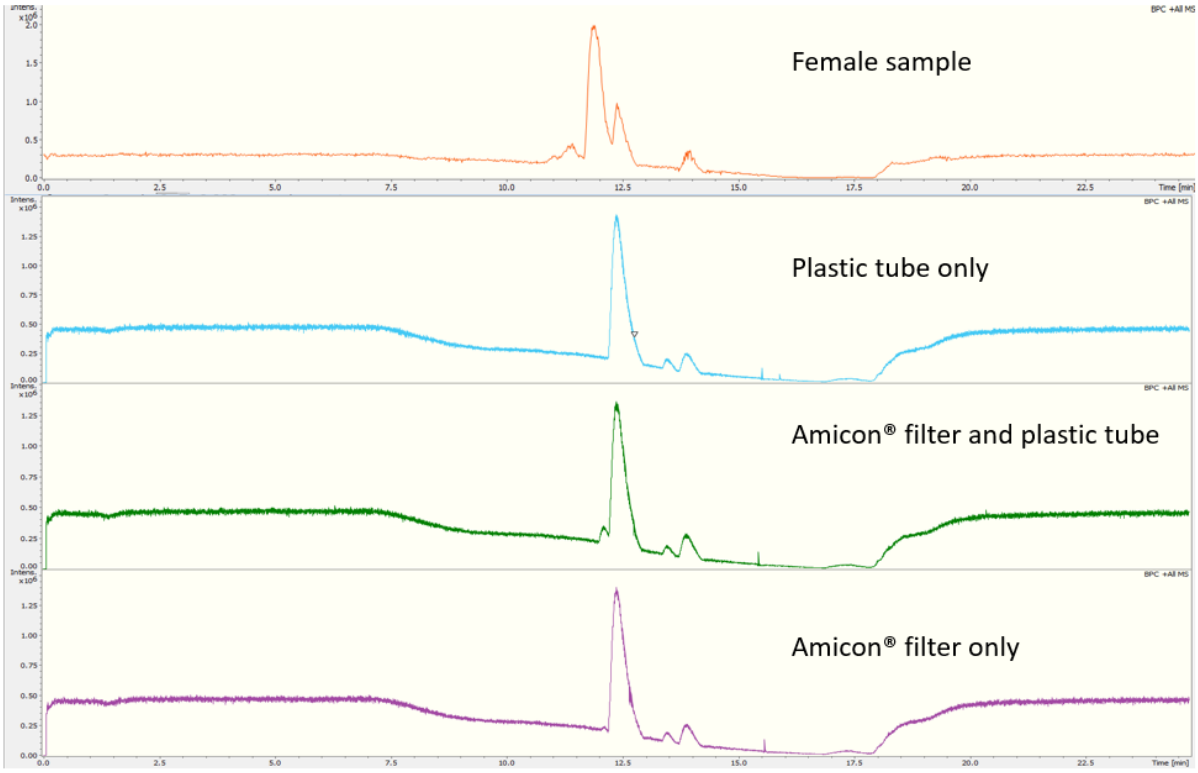

Figure 12. Chromatogram in BPC (most intense ion showing) with the sample in red, the test in plastic tubes only in blue; the test with Amicon® filter only in purple and in green the test with the full method and no sample (plastic tubes and Amicon® filter).

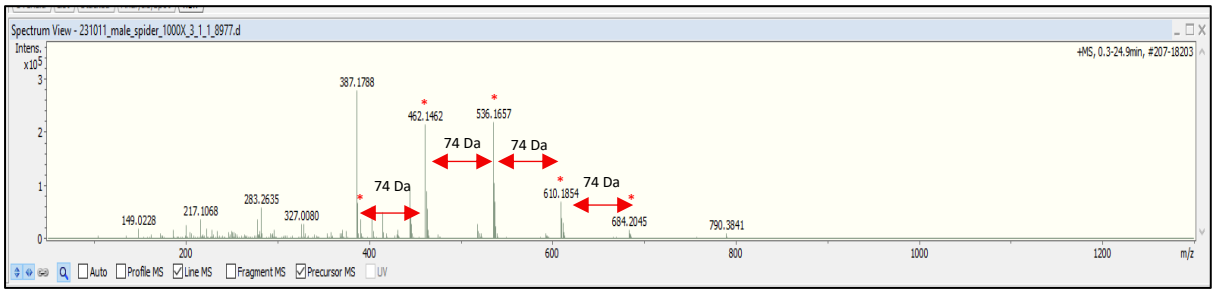

Figure 13. MS spectra of *Steatoda nobilis* extract after the first protocol for the preparation of the sample. All the detected peaks are contaminants, and none come from the actual sample. The peaks marked by a red star (*) are peaks from a dimethylsiloxane polymer.

Improving the extraction of the metabolites. Due to different problems met with the first samples, the protocol had to be adapted. After crushing the samples, the powders were collected in glass vials instead of plastic tubes to prevent any contamination from the storing. The remaining traces of powder adhering to the mortar were retrieved using 800 µL of MeOH/H_2O (80/20, v/v). The samples underwent a 15 min sonication process using a Branson 1510® ultrasonic cleaner (Branson, USA) then centrifuged at 7200 G for 2 min in an Eppendorf® 5415 R centrifuge (Eppendorf®, Belgium). The supernatants were collected and recovered in a glass tube and 500 µL of a new fresh solution of MeOH/H_2O (80/20, v/v) was added to the pellet. This operation was repeated 3 times for each sample.

The Amicon® filtering step was demonstrated to be a source of contamination and was consequently abandoned. Indeed, this step was an additional security to avoid any clogging of the column, not inspired from reference studies, and removing it does not constitute an issue. Once the supernatants

were collected, the samples were dried using a SpeedVac®. To prepare the samples for the injection in LC-MS/MS, they were diluted in 1 mL of H_2O/ACN (99/1, v/v). As discussed above, as it was impossible to evaluate the concentration of extracted metabolites in our samples and to avoid any overload of the LC column, additional dilutions of 1:1000, 1:100 and 1:10 were prepared. The most diluted one was first injected and the results are described below.

Following this modification of the protocol, the ensuing results displayed marked improvements. The blank exhibited notable distinctions from the sample, and the chromatogram and MS spectra revealed an increased presence of ions (Figure 14). The revised method successfully identified a total of 682 peaks across male, female, and blank samples, employing a threshold intensity of 2,500 to ensure peaks were 3 times more intense than the noise. Among these, 237 peaks were consistently present in all three instrumental replicates of the female sample, with 177 peaks found consistently in all triplicates of the sample and absent in the blank (data are proposed in the annex in table 1).
However, a notable concern persisted, as 21.1 % of the peaks (50 peaks) in the female sample and 31.1 % (55 peaks) in the male sample also appeared in the blank, indicating contamination from the instrument or solvents used. This underscores the ongoing challenge posed by contamination in the analysis of this sample type using the laboratory's instruments. Despite this, a promising observation emerged: certain peaks were "specific" to the blank and did not appear in the *Steatoda nobilis* spectra. This led to the hypothesis that the sample molecules may possess a higher ease of ionization. If these molecules engage in a competitive ionization process, the spider analytes would exhibit preferential charging over the contaminants. Consequently, the contamination's impact on the mass spectra appears to be less severe than initially anticipated.

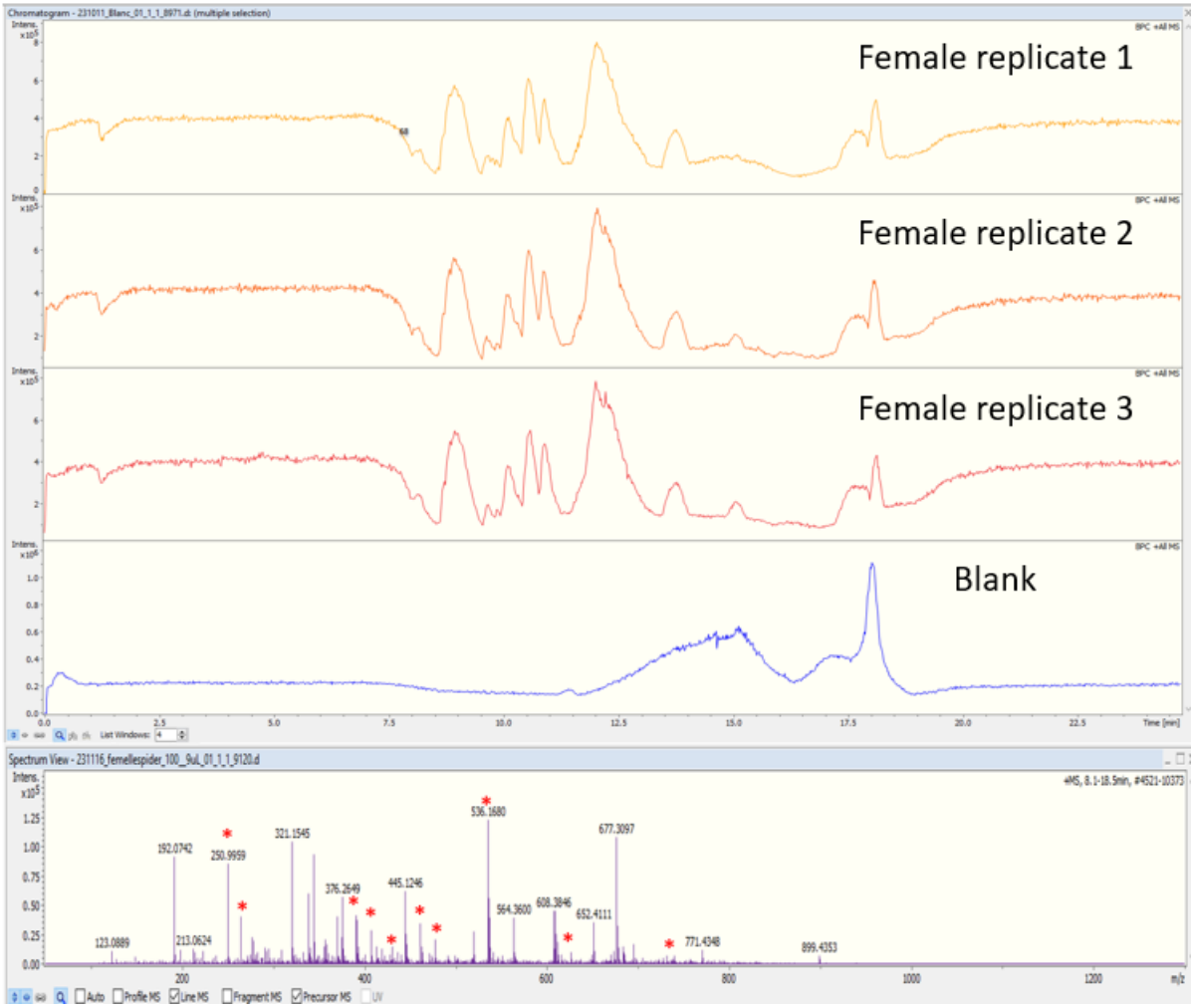

Figure 14. Illustration of the contamination during the LC-MS/MS experiments. In yellow, orange and red an instrumental triplicate chromatogram in BPC and MS spectrum of a female *Steatoda nobilis* extract sample with the main contaminants shown with red stars. In blue, the chromatogram in BPC and MS spectrum of the empty analysis that was sent before the analysis.

Analyzing the similarities between the biological sample, 23.2 % of the signals (78 peaks) are shared between male and female spiders. Conversely, 29.5 % of the signals (70 peaks) are unique to the females, and 17.0 % (30 peaks) are specific to the males (Figure 15). It is crucial to note that these percentages are calculated with consideration for instrumental triplicates. In practical terms, a specific peak attributed to the males (for example) must be detected in each of the three replicates corresponding to the male, and never detected in the female samples. This stringent criterion applies to male and female samples as well, elucidating why the total number of gender-specific peaks and shared peaks do not sum up to the overall number of detected peaks. The number of peaks specific to male (30) and female (70), and shared between male and female (78), may appear quite low but, as nothing has already been done on spider metabolomes, this information is difficult to evaluate. It is true that the nature of the UHPLC column, here a hydrophobic phase (reversed phase), limits the detection of the molecules belonging to a range of polarity between low and mid. The highly polar metabolites are not retained by the column and are lost into the waste. For a more exhaustive analysis, the use of a HILIC® column could be invoked as a second analysis. This phase allows for the examination of more polar metabolites, providing a more global view of the spider metabolome. This represents a clear perspective of the work.

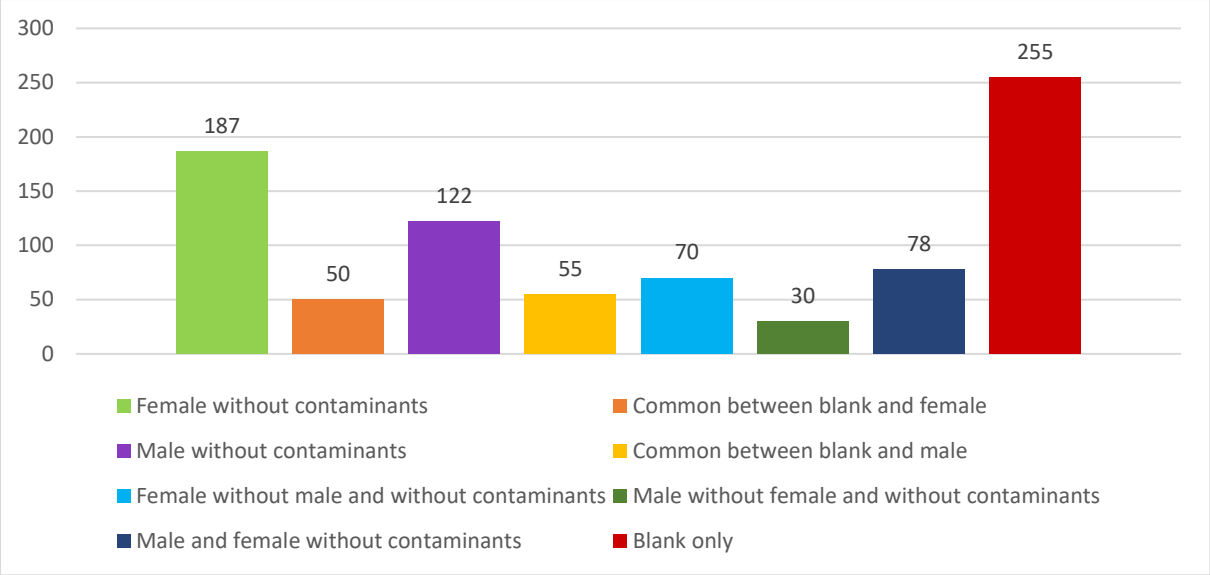

Figure 15. Histogram of the quantity of peaks for, in order, the female sample without contaminants, the peaks in common between the female sample and the contaminants, the peaks for the male sample without contaminants, the peaks in common between the female sample and the contaminants, the peaks present in the female sample not the male sample and without contaminants, the peaks present in the male sample not in the female sample and without contaminants, the peaks in common between male and female samples without contaminants and the peaks corresponding to the contaminants (named "blank only").

One of the advantages of the TIMSTOF-Pro 2 spectrometer is its ability to perform tandem mass spectrometry (MS/MS). The principal objective was to confirm the identification of ions identified only based on their exact mass in LC-MS, but also and more conveniently in the MSI experiments. The analysis of fragmentation patterns is indeed a gold mine to either validate or establish metabolite identification. The envisioned ideal analytical protocol involved the systematic retrieval of molecular information, elucidation of their fragmentation pathway by the help of a database, followed by a meticulous comparison with the MS/MS data. However, this approach encountered substantial challenges attributed to the paucity of information within existing databases concerning the specific taxonomic group under investigation, i.e., spiders. This dearth of information significantly impeded the identification process. Consequently, the manual curation of all spectra became imperative, an intricate and time-consuming task. The inefficiency of this manual process was exacerbated by the prevalent presence of contaminants, complicating the analysis and rendering it susceptible to potential errors.

Numerous molecules detected have however been identified as phosphatidic acids containing primary or quaternary amines, which make them more easily detectable in positive ion mode. Consequently, the charge of the ion is almost always localized on the amines and close to the neutral phosphate group. In addition, given that the fragmentation of these molecules predominantly occurs near the phosphorus, the charge always appears on the same part of the fragments (Figure 16).

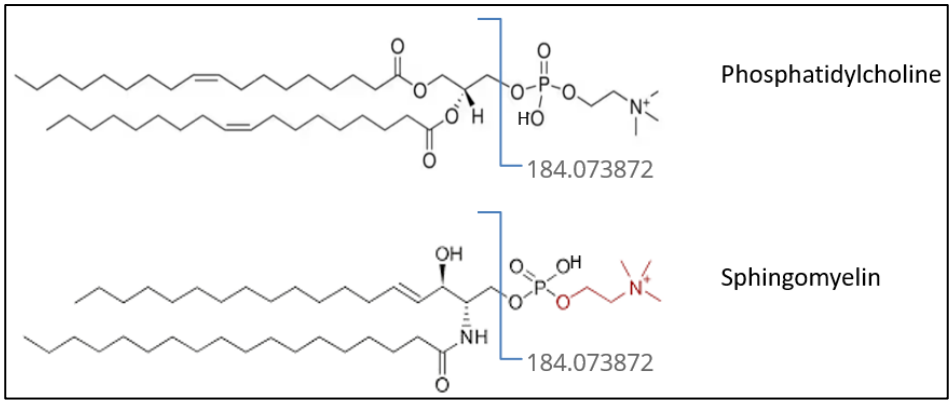

Figure 16. Example of the fragmentation pathway of a phosphatidylcholine (PC(18:1(9Z)/18:1(9Z))) and a sphingomyelin (18:0 SM).

This commonality in fragmentation patterns results in frequently observed and comparable MS/MS spectra, limiting the information yield for comprehensive analysis as shown in Figure 17. In that Figure, the fragments that can be seen are the 184 which corresponds to the phosphocholine fragment and the 589 which is the $[M+H -H_2O]^+$.

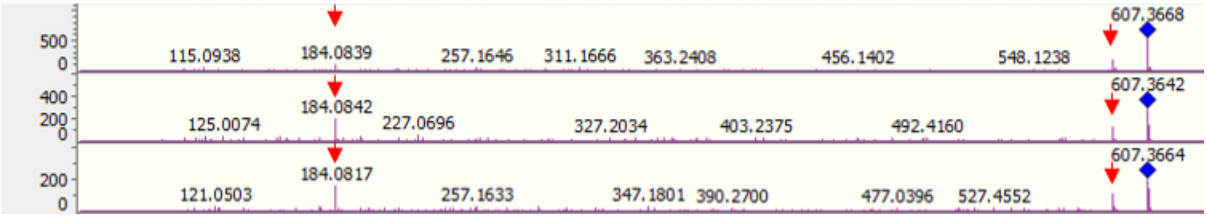

Figure 17. MS/MS fragmentation spectra of a phosphatidylcholine. In blue is the ion fragmented (same ion for the 3 MS/MS), in red are the two ions that are common to the three fragmentation spectra.

II. MALDI MSI results

Optimizing Mass Spectrometry Imaging for Whole-Body Analysis of *Steatoda nobilis*: Experimental Results and Insights.

Once the sample preparation is set up, the optimization of a MALDI-MSI method reveals new challenges mainly associated with time and data processing. Each analytical test requires a substantial investment of time, ranging from 20 to 60 hours per image. Furthermore, the generated data files are extensive, reaching up to several TB per file, depending on the number of pixels and the desired mass spectrum resolution desired by the operator. The intrinsic laboratory computing resources may also represent a limitation for swift processing of such large datasets, impacting the efficiency of tasks like opening, exporting, and submitting data for analysis, which can take up to several days. Additionally, the sizable files pose limitations as they are mostly not usable with classical software tools, necessitating data reduction and transformation to comply with these imposed requirements. These constraints collectively extend the duration of a single test, easily spanning several weeks from sample preparation to analysis, posing challenges for the practicality of this approach in the context of a master's thesis project. The optimization process also addressed section thickness, aiming to maximize molecule detection by the instrument and solve issues, such as instrumentation failures or poor results. In this context, the complexity of doing MSI for a whole-body spider is clearly high, from the sample

preparation (as discussed above) to the data treatment. Acquiring an image of the spider metabolome directly from tissue slices constitutes a real analytical challenge that necessitated extensive optimization and testing to establish a robust imaging protocol.

Even after several days of work, some results may appear disappointing. Two imaging runs provided valuable insights despite the absence of anticipated results. This is illustrated by the Figure 18, with two images, one of a 16-µm section slice of a female *Steatoda nobilis* that has been acquired using HCCA as the matrix and one of a 25-µm section slice of a male that was acquired using DHB as a matrix. On Figure 18, the images produced by the instrument are overlapped with the histological slices. The data from the instrument was subtracted from the image, leaving only the zones that can be seen on the MS imaging run. The image of the female recovered with HCCA matrix only revealed a few pixels containing ions, strongly deviating from classical expectations for a typical imaging run. Even if the tissue slice was perfectly deposited on the ITO slide and covered by an adapted layer of matrix, no metabolite was detected and only ions coming from the matrix were present. A tentative hypothesis was imagined to explain this behavior: the sample might have been too thin, preventing enough extraction and ionization of metabolites to be detected by the spectrometer, or even too thick, insulating the sample and avoiding abundant ion extraction. A trial-and-error optimization process for section thickness, aiming to maximize molecule detection and address various issues, revealed another challenge. The laser, even if it is designed for imaging purposes, can be too rough and may damage the sample. Helped with the vacuum, the laser can indeed degrade the sample to the extent that spider organs were ejected from the slides into the instrument, destroying any hope of generating an interpretable image. After various experimentations, the optimal thickness for such spider samples was determined to be 25 µm, ensuring not only organ retention on slides but also providing optimal ionization.

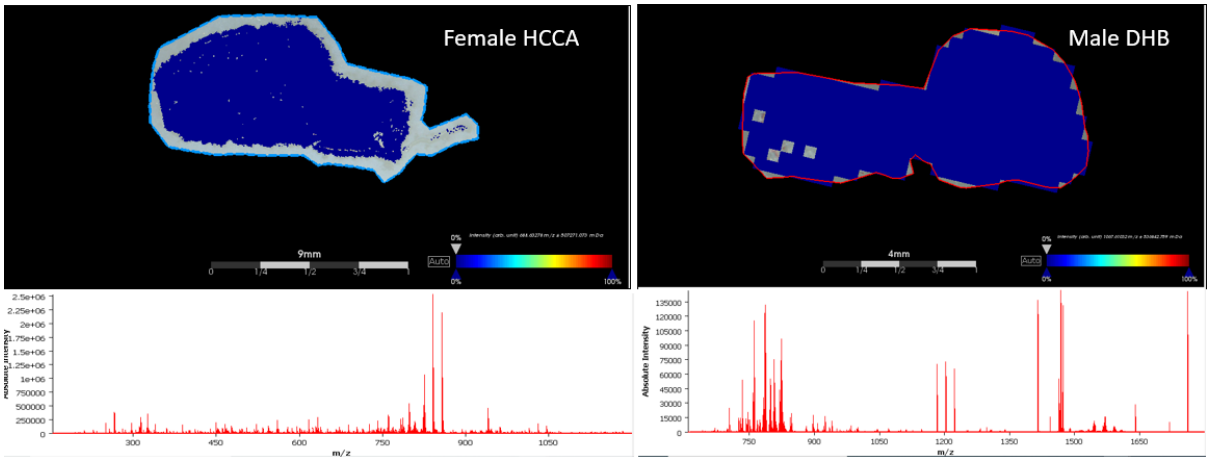

Figure 18. Mass spectrometry MALDI Imaging run of *Steatoda nobilis* that yielded no results. On the right is a female sample covered with HCCA matrix and on the left is a male sample covered with DHB matrix. Pixels with an MS spectra are in grey, blue is the original selected zone and under is the MS spectra linked with the image.

After the optimization of the thickness, four images were acquired. Female and male *Steatoda nobilis* slices where imaged using either HCCA, powerful for detecting small compounds, or DHB matrix, able to detect small to medium-sized compounds. Different bioinformatics solutions were employed to demonstrate the potential of metabolomic analysis through MSI (SCiLS® from Bruker, the home-made MSKF and the web interface Metaspace®). Each of these tools provides a different degree of information, explaining why their combination was imperative to comprehensively extract data from the images and to accurately evaluate them by the mean. As a reminder, SCiLS® is the dedicated tool

provided by the spectrometer manufacturer to assess the quality of the results, to get an overview on the average mass spectrum and to generate images from selected peaks or range of m/z. As explained in the Material and Method section, Mass Spectrometry Kendrick Filter (MSKF) software is used to classify the ions into structural families. It also allows to generate images of any selected zone of the Kendrick plot KMD = f(m/z). Doing so, images of metabolite families are easily reconstructed, which is not possible for SCiLS®. Finally, Metaspace®, a web-interface, allows the identification of the metabolites, based on their exact mass, provided by the impressive property in terms of mass accuracy measurement of the FT-ICR mass analyzer.

Data analysis guided by SCiLS® software. The first analysis that was performed on the images was a segmentation, with the aim to find all the zones visible for each image. This is depicted in Figure 19 and 20, where the segmentation reveals distinct zones on the spider. These zones were then identified using anatomical drawings and histological sections of the spider. Identified zones clearly encompass the ovaries, vascular system, nervous system, silk glands, and the brain of the spider. These zones are represented on a histological section on Figure 19, where they are circled in colors (ovaries are orange, the brain is yellow, the heart is dark blue, the abdomen cavity is light blue and the silk glands are red). This process was also done for the other samples and the result of the segmentation is shown in Figure 20. The segmentation serves primarily to evaluate which parts of the sample stand out and to anticipate the expected organs or systems. However, a limitation of this method lies in the absence of detailed information on the detected molecules explaining the segmentaion and their relative intensities. Consequently, this tool serves more as an informative preliminary step to sample analysis, assessing the relevance and utility of spatial information and aiding in localization.
The software's outcomes include the extraction of information on whether molecules specific to certain zones or organs were identified and the spatial distribution of these zones within the images.

Although the mass spectra can also be analyzed on the SCiLS software, there is no tool to find interesting ions. To obtain images, the signals have to be taken one by one to find which ones are specific to certain zones or organs. Since these images contain thousands of peaks, this strategy is not adapted and other, more optimized methods have to be found to analyze these images. The approach based on the Kendrick mass defect looks promising and is detailed in the section below.

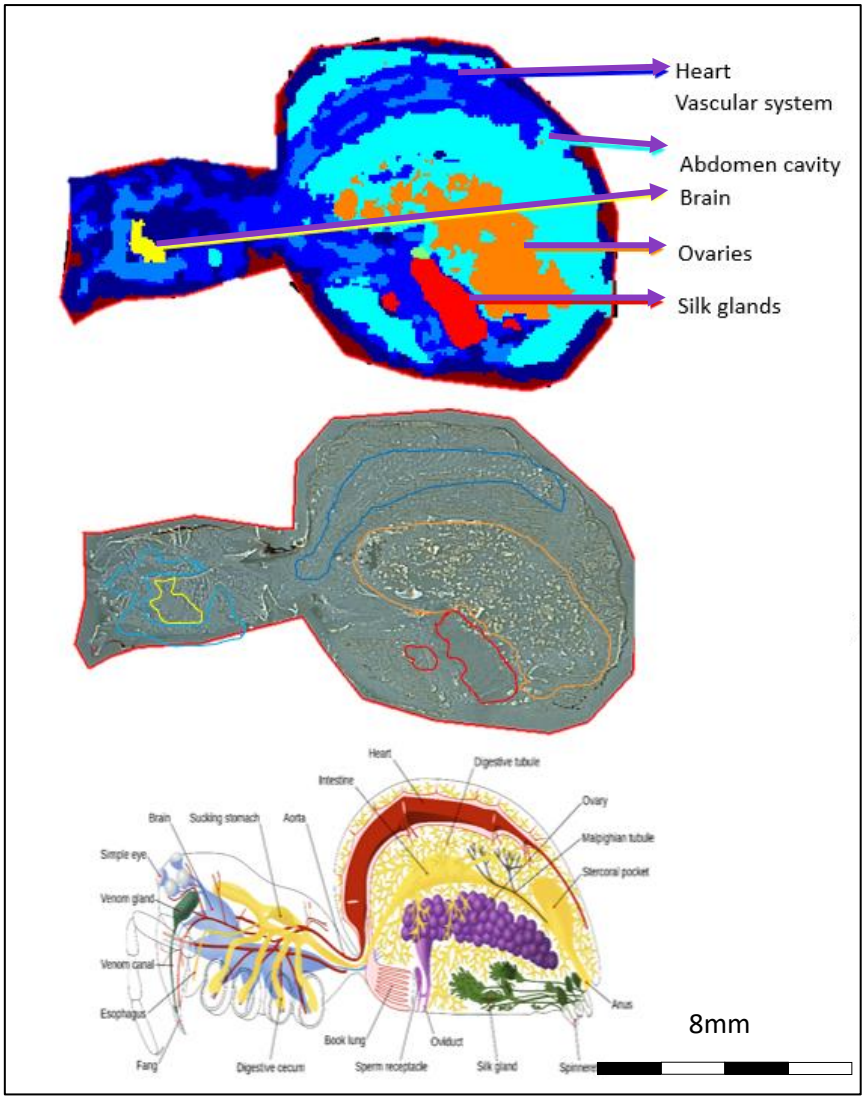

Figure 19. Image of the segmentation made by SCiLS® on a the MALDI MSI female spider covered with HCCA matrix. On top, the segmentation detected with the different zones. On the bottom, the slice from which the image was taken with the zones drawn. Segmentation Analysis in MALDI MSI of Female *Steatoda nobilis* Spider using HCCA Matrix: SCiLS®-Generated Image, Zone Detection, and Slice Visualization

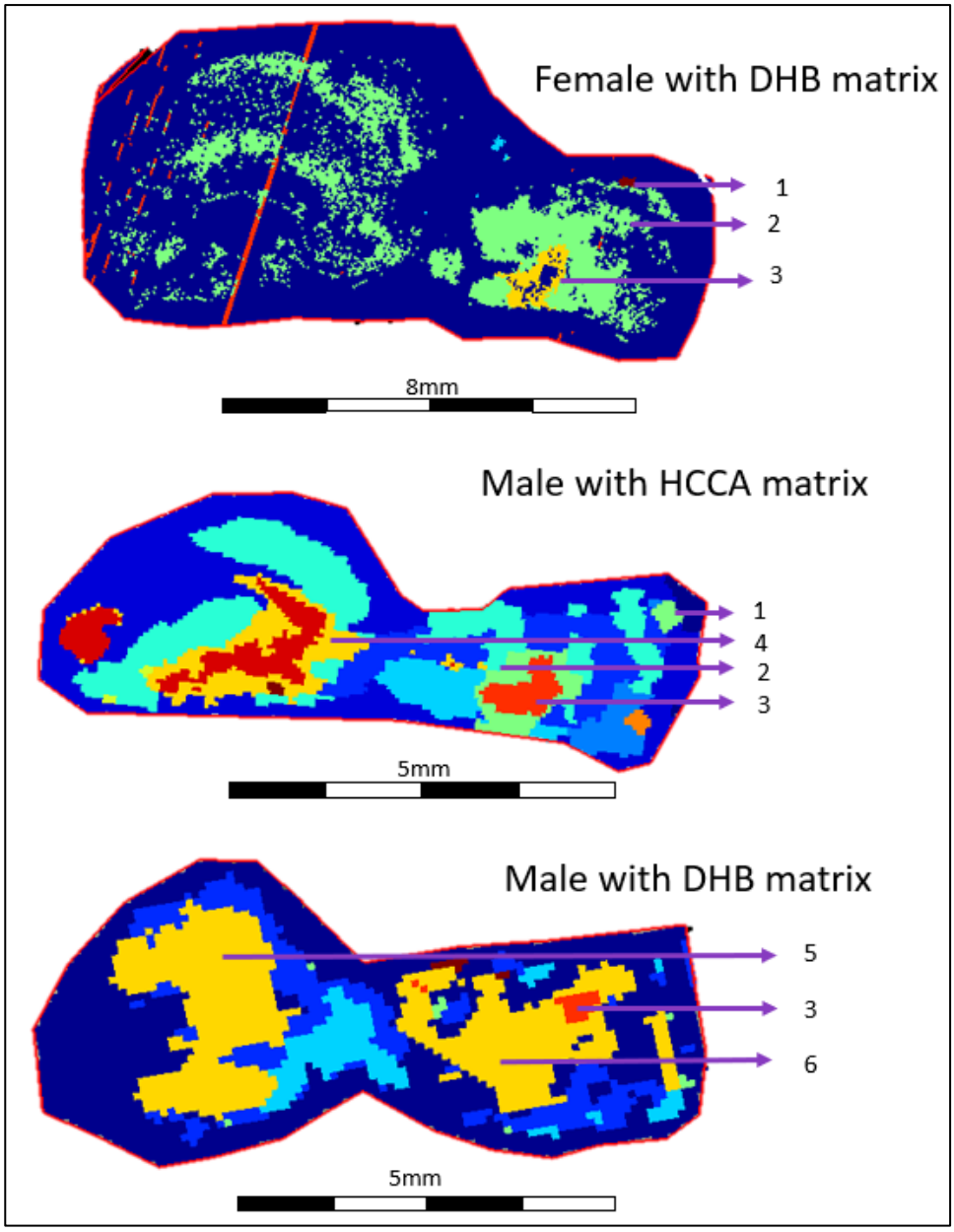

Figure 20. Segmentation Analysis of MALDI MSI Experiment on a female *Steatoda nobilis* Spider using DHB Matrix, on a male spider covered with HCCA matrix and on a male *Steatoda nobilis* using DHB Matrix: SCiLS®-Generated Image, Zones, and Corresponding Slice Representation. On the images, 1 corresponds to the eyes, 2 to the vascular system, 3 to the brain, 4 to a cavity in the abdomen, 5 to the abdomen and 6 to the head of the spider.

Data analysis using Mass Spectrometry Kendrick Filter (MSKF). Each of the images was transformed from an ".imzml" into a ".ick" file using the built-in tool of the software (specific format for this software) to allow it to be opened in MSKF software. As a reminder, MSKF is a Kendrick software which generates plot of Kendrick Mass Defect (KMD) in function of the m/z of the ions (Figure 21). This transformation is performed with CH_2 as a base unit to align some classes of metabolites, but mainly for lipids. As shown on this figure, the peaks are transformed into dots that are grouped in kind of clouds, representing mostly structural families of compounds. Within a family, some peaks are horizontally aligned, indicating that they differ only by their number of CH_2, while some are diagonally aligned, indicating that they differ only by their number of unsaturation (difference of 2 hydrogen atoms in mass).

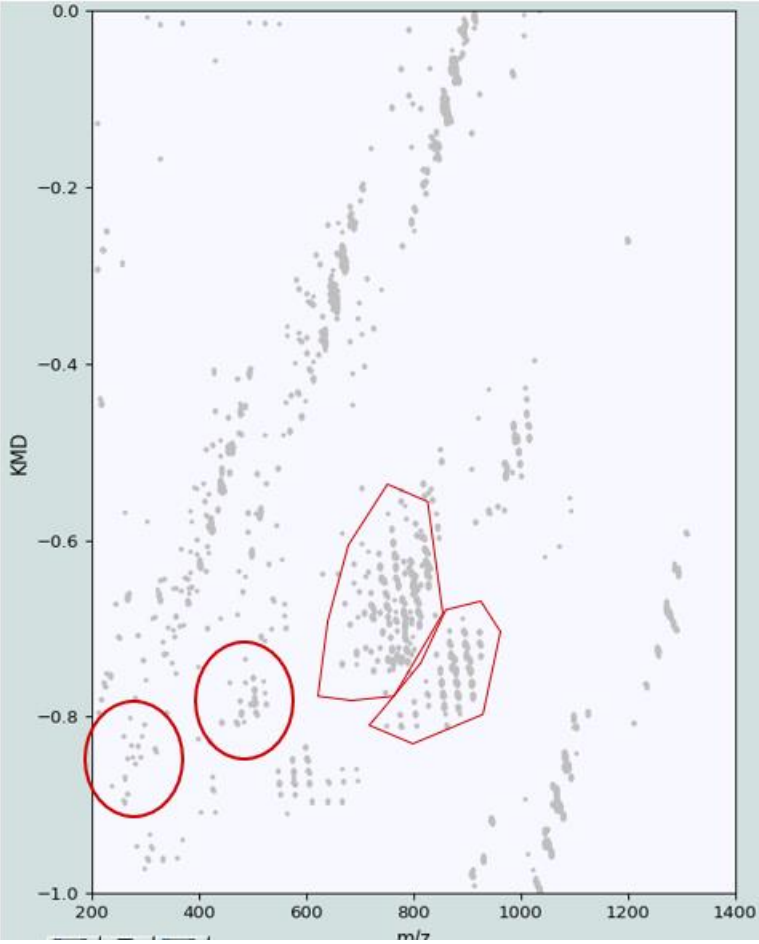

Figure 21. Kendrick plot obtained in MSKF for MSI on a sagittal slice of *Steatoda nobilis* female spider with HCCA matrix. The interesting zones investigated during this thesis are shown in red. Image generated by MSKF.

Data analysis with MSKF drove to the detection of interesting zones that stood out from the rest of the sample. Indeed, in Figure 21, some zones with large families or with ions exhibiting peculiar behaviors were studied. Figure 22 details the results obtained for the area delimited on the Kendrick plot by KMD [-0.8; 0.65] and m/z [750; 950]. It shows a group of ions aligned horizontally and diagonally and which appear to be part of the same family. All these ions are all located in the cuticle of the spider. In Figure 23, the zone of interest is delimited on the Kendrick plot by KMD [-0.8; 0.7] and m/z [450; 500]. This shows a smaller group of ions belonging to the same family that are located in the ovaries of the spider. The next interesting zone, studied in Figure 24, is delimited on the Kendrick plot by KMD [-0.7; 0.65] and m/z [750; 950]. It shows that these compounds are present in the vascular of the spider. Figure 25 finally, shows two ions which do not belong to any family but that are the only ones present in what appears to be the silk glands of the spiders. Since no other ion is present in that zone, these two metabolites seem to have a special role in the silk glands but the identification cannot be made using this software.

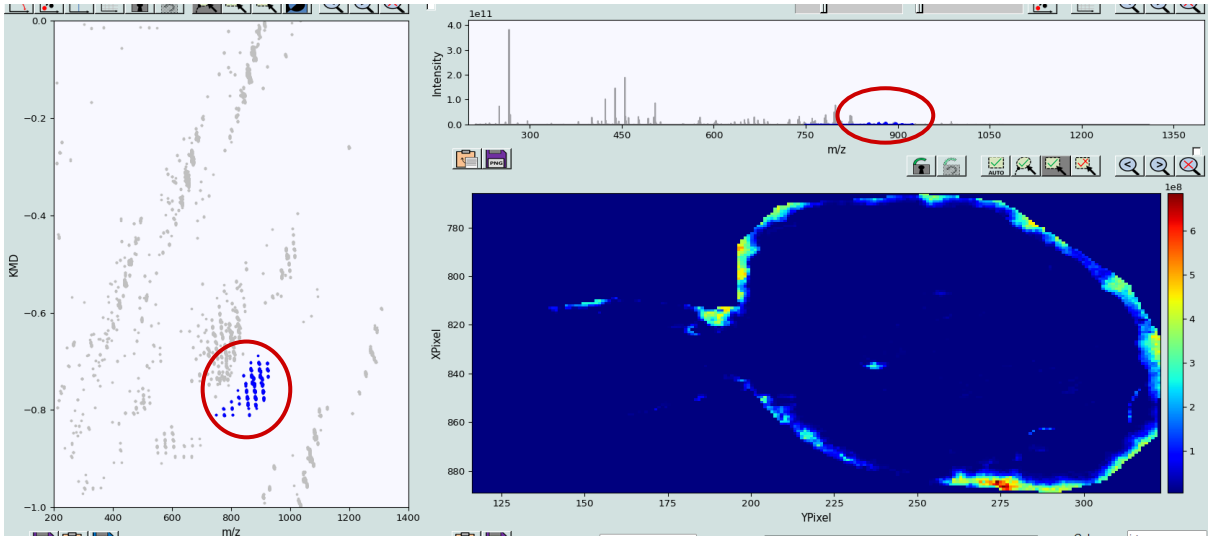

Figure 22. Image obtained in MSI on a sagittal slice of *Steatoda nobilis* female spider with HCCA matrix in MSKF, the zone highlighted seems to be the cuticle of the spider. On the left is the Kendrick plot, on top is the MS spectra and on the bottom is the image of the selected ions. Selected ions appear in blue and are listed on the right.

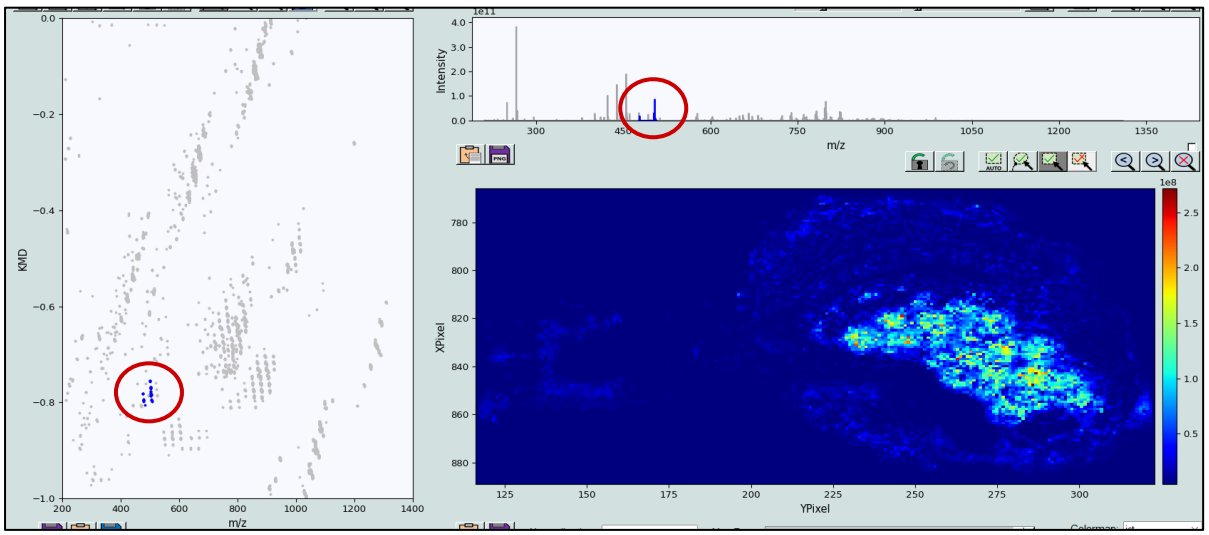

Figure 23. Image obtained in MSI on sagittal slice of *Steatoda nobilis* female spider with HCCA matrix in MSKF, the zone highlighted seems to be the ovaries. On the left is the Kendrick plot, on top is the MS spectra and on the bottom is the image of the selected ions. Selected ions appear in blue and are listed on the right.

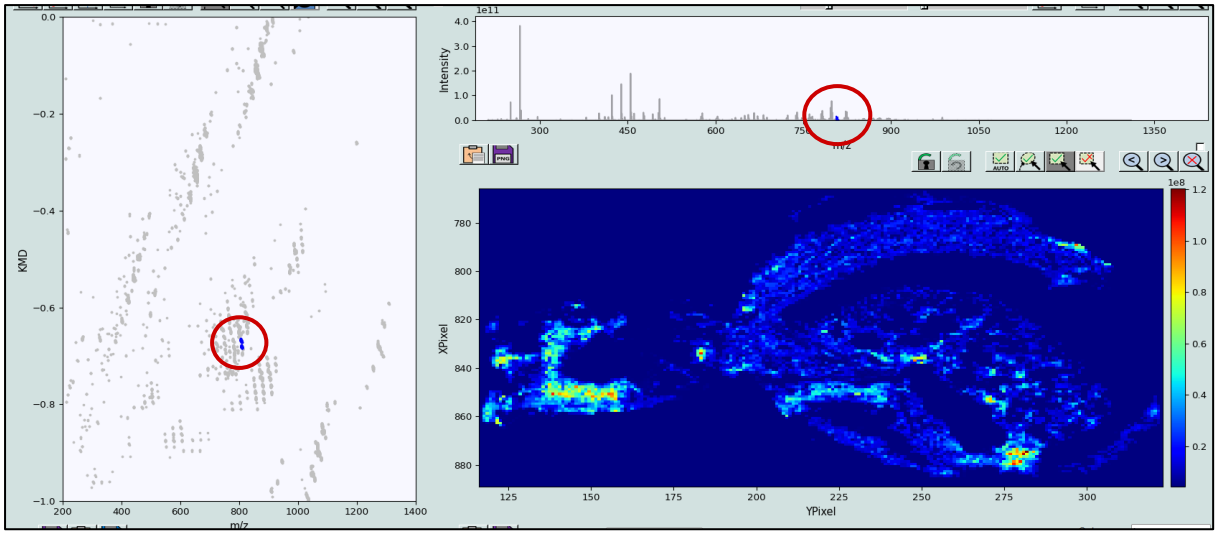

Figure 24. Image obtained in MSI on a sagittal slice of *Steatoda nobilis* female spider with HCCA matrix in MSKF, the zone highlighted seems to be the vascular system. On the left is the Kendrick plot, on top is the MS spectra and on the bottom is the image of the selected ions. Selected ions appear in blue and are listed on the right.

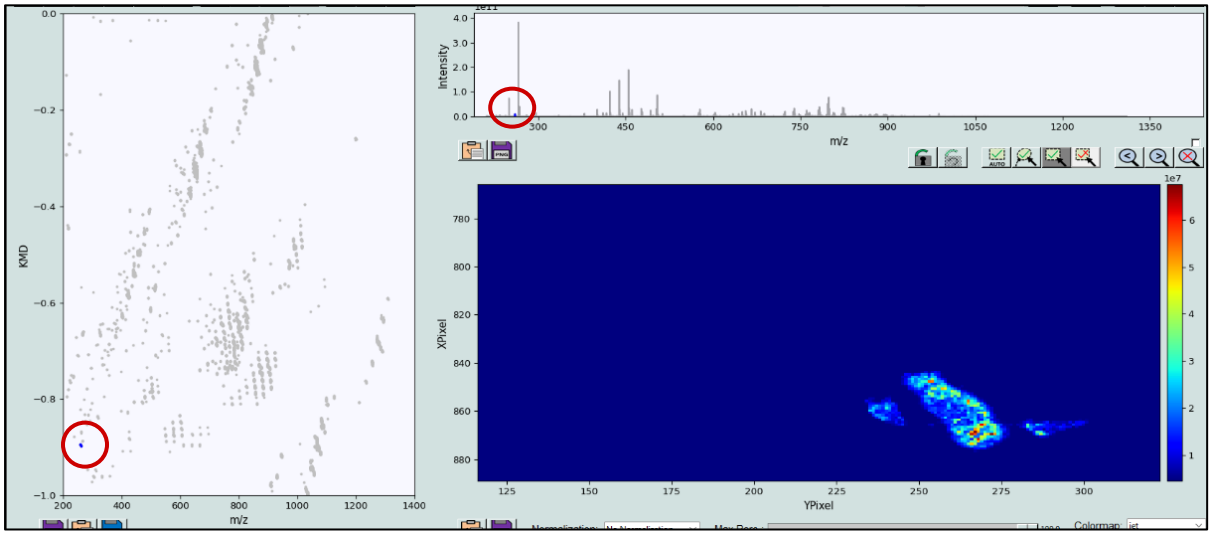

Figure 25. Image obtained in MSI on saggital slice of *Steatoda nobilis* female spider with HCCA matrix in MSKF, the zone highlighted seems to be the silk glands. On the left is the Kendrick plot, on top is the MS spectra and on the bottom is the image of the selected ions. Selected ions appear in blue and are listed on the right.

As we see, SCiLS allows us to generate images from single ions, and the segmentation allows us to find interesting areas rapidly. However, no link can be made between these zones and the molecules detected. MSKF, in contrast, allowed us to classify the molecules into different families based on their Kendrick mass defect and to generate images for these families of metabolites. But the identification of these molecules is still missing, this information was brought by Metaspace®, detailed in the section below.

Metaspace®. Metaspace® is a tool that leverages databanks for the identification of molecules from experiments, based on exact masses. The interest of acquiring images with an FT-ICR spectrometer appears then as a real advantage.

The composition of samples used to populate the databanks is a critical factor. For instance, the absence of metabolites coming from studies on arthropods is a dearth of specific ions associated with

these species. Consequently, the veracity of the information obtained is contingent upon the concordance between ions present in the images and those cataloged in the databanks, leading to potential instances of undetected ions and misidentifications. Moreover, the false discovery rate (FDR) in Metaspace® is confined to four values: 5 %, 10 %, 20 %, and 50 %. While the 5 % FDR engenders a commendable confidence level, a considerable number of ions were detected at a 10 % FDR, undermining the reliability of identifications. In a bid to bolster the confidence level of results, data derived from the SCiLS®, MSKF, and the LC-MS/MS were incorporated to corroborate the identifications made by Metaspace®. However, one can argue that most metabolites are somehow universal and belong to the same kind of molecules (lipids, sugars, amino acids,…) So, although our approach may miss some unknown specific arthropod metabolites, most of the identifications should be exact and describe (at least partially) the metabolome of *S. nobilis*.

Table 2 shows four examples of the type of analysis that can be made using Metaspace®. These four molecules were analyzed by taking their m/z, their localization on the image, their identification (made by Metaspace®), the structure of the molecule (also given by Metaspace®) and the role of the identified molecule(s) (and isomers).

The first molecule was identified as Kynurenic acid and is localized in the nervous system of the spider. This molecule plays an important role in the formation of a neuroprotective molecule (Tóth *et al.*, 2021). It is therefore logical to find it in the nervous system and the brain of spider. The localization reinforces the identification made by Metaspace®.

The second example is the hexanoylcarnitine which is found in the silk glands of the spider. Since the role of hexanoylcarnitine is to transport fatty acids for energy metabolism[2], finding it in the silk glands is not surprising. Indeed, the production of silk requires enormous amounts of energy (Tanaka, 1989), which might explain why this molecule was found in these peculiar organs.

The third molecule is a sphingomyelin that was detected in the nervous system of *Steatoda nobilis*. Since sphingomyelins are components of myelin sheaths that cover the nerves (Goñi, 2022), we can assume that the identification from Metaspace® is also pertinent.

The last molecule is a triglyceride that was found, like all triglycerides identified by Metaspace®, in the cuticle of the spider. Although there is no known reason as to why triglycerides are found on the cuticle of the spider, since 42 different triglycerides were found in the same zone, we can safely assume that, in the case of *Steatoda nobilis*, finding these molecules in the cuticle is normal and that the identification is correct. Further investigations are needed to have a deeper understanding of this observation.

[2] https://www.smolecule.com/products/s617495

Table 2. Example of the list of molecules identified using Metaspace® for the MALDI analysis of a female *Steatoda nobilis* with HCCA matrix.

Ion (m/z)	Image and zone	Metaspace identification and potential isomers	Structure	Role
228.0058	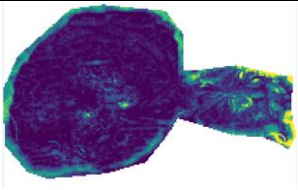 Brain and nervous system	Kynurenic acid (no isomers)	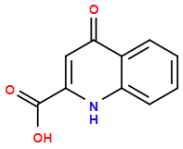	Precursor to a neuroprotective agent (Tóth *et al.*, 2021)
260.1856	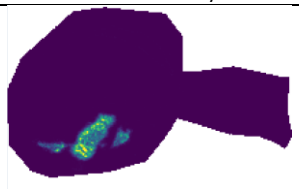 Silk glands	Hexanoylcarnitine (no isomers)	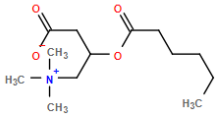	Transport of fatty acids for energy metabolism[3]
725.5568	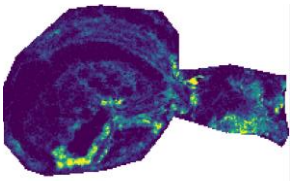 Nervous system	Sphingomyelin SM(d18:0/16:1(9Z)) or SM(d18:1/16:0)	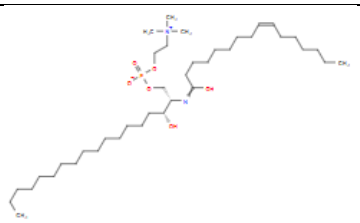 or 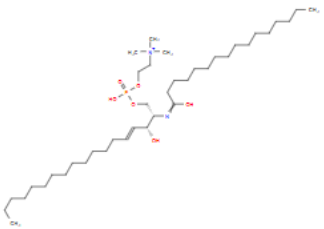	Used in myelin sheath protecting the nerves (Goñi, 2022)
879.7412	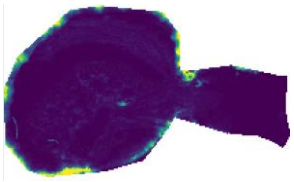 Cuticle	Triglyceride TG (16:0/18:1(11Z)/18:1(9Z)) or isomers TG (18:1(11Z)/16:0/18:1(9Z)) TG (16:1(9Z)/16:1(9Z)/20:0) TG (16:0/18:1(9Z)/18:1(11Z)) TG (16:0/16:1(9Z)/20:1(11Z)) TG (16:0/18:1(11Z)/18:1(11Z)) + 8 others	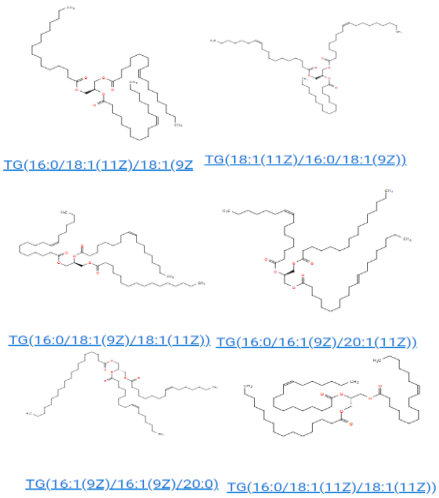 TG(16:0/18:1(11Z)/18:1(9Z TG(18:1(11Z)/16:0/18:1(9Z)) TG(16:0/18:1(9Z)/18:1(11Z)) TG(16:0/16:1(9Z)/20:1(11Z)) TG(16:1(9Z)/16:1(9Z)/20:0) TG(16:0/18:1(11Z)/18:1(11Z))	Used as fat for the storage of energy (Wiesner & Watson, 2017)

[3] https://www.smolecule.com/products/s617495

The full data obtained from Metaspace® is compiled in the supplementary information[4] in tables 2-5 and on Figures 1-27, but the data was not thoroughly checked so some identification might be wrong. However, it is important to note three things: isomers cannot be distinguished without efficient MS/MS or ion mobility data, the Δm/z (ppm) might be biased (see below) and the MS/MS identification can only be used as a higher confidence in the identification. For the identification in MSI, we only have access to the exact mass which prevent any distinction between the isomers of the same molecules.

In the case of the Δm/z (ppm), the problem arises from the fact the data was centroided, which means the large peaks are reduced, in theory, to a peak with infinitely small width (shown in Figure 26). Unfortunately, in the case of large, non-symmetrical peaks, each peak can be separated into multiple peaks. This is supposed to be resolved by the recalibration of the image, which merges the divided peaks into a single peak. However, this process led to pixels being merged and resulted in empty rows of pixel with part of the data being unusable.
So, in this case, since Metaspace® requires centroided peaks to function properly, the peak that was taken by the software is the one with the best match for the identification and not the m/z corresponding directly to the detected ion. The program treating the data afterwards does not know if the centroided peaks are related to the maximum of a single peak, or to artefacts ones. This introduces a bias in the Δ(m/z) since the closest one to the mass of the identified ion will be taken by the program. This problem does not have an important impact on the identification of the molecules, it just means that we cannot fully rely on the Δ(m/z) for the analysis. Nevertheless, the Δ(m/z) can still be useful to discriminate between likely or unlikely match, like for example, if the Δ(m/z) is superior to 5, then we can be sure the molecule is misidentified.

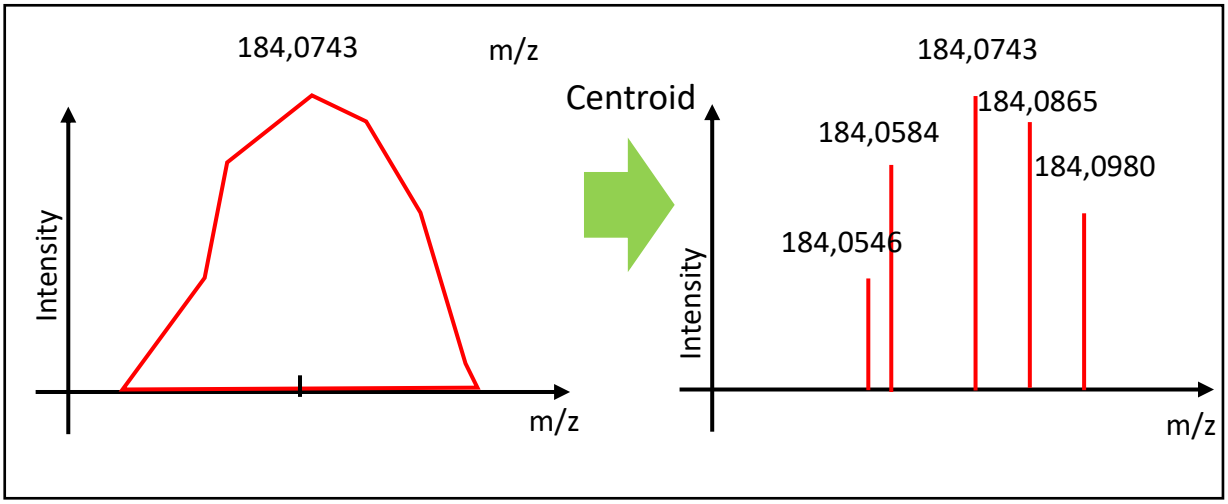

Figure 26. Illustration with a theoretical peak of the impact of centroiding on peak integrity and ambiguity in subsequent data processing. An example of what happens to a peak when centroided. The program treating the data afterwards does not know if the peaks are related or not and which one corresponds to the real peak.

The analysis of phosphatidylcholines, abundant in our samples, presents a challenge. This difficulty arises from the MS/MS process, wherein fragmentation occurs within a range of approximately one m/z around the detected ions. Consequently, numerous ions of varying masses can undergo fragmentation simultaneously, if they are detected within the same m/z .

[4] Master thesis supplementary information.docx

A total of 374 distinct molecules were identified across the analyzed samples with Metaspace®. The specific data is shown in Figure 28, where for the female sample coated with HCCA matrix, 183 molecules were detected within the mass range of 228 to 973. In the case of the same sample but coated with DHB this time, 110 molecules were identified within the mass range of 675 to 1043. For the male sample coated with HCCA matrix, 60 molecules were detected spanning the mass range of 228 to 1092. Meanwhile, for the male sample covered with DHB matrix, 293 molecules were identified within the mass range of 522 to 925. Upon closer examination, it is shown that 67 molecules are shared between the two female samples, whereas only 36 molecules exhibit commonality among the male samples. Collectively, only 13 molecules are found to be common across all four samples. While this might suggest a potential lack of reproducibility between samples, it is essential to acknowledge the constraints imposed by the limited sample size and the inherent inadequacies of existing databanks, particularly in addressing the intricacies of arthropod analysis (full data obtained from Metaspace® is compiled in the supplementary information[5] in tables 2-5 and on Figures 1-27).

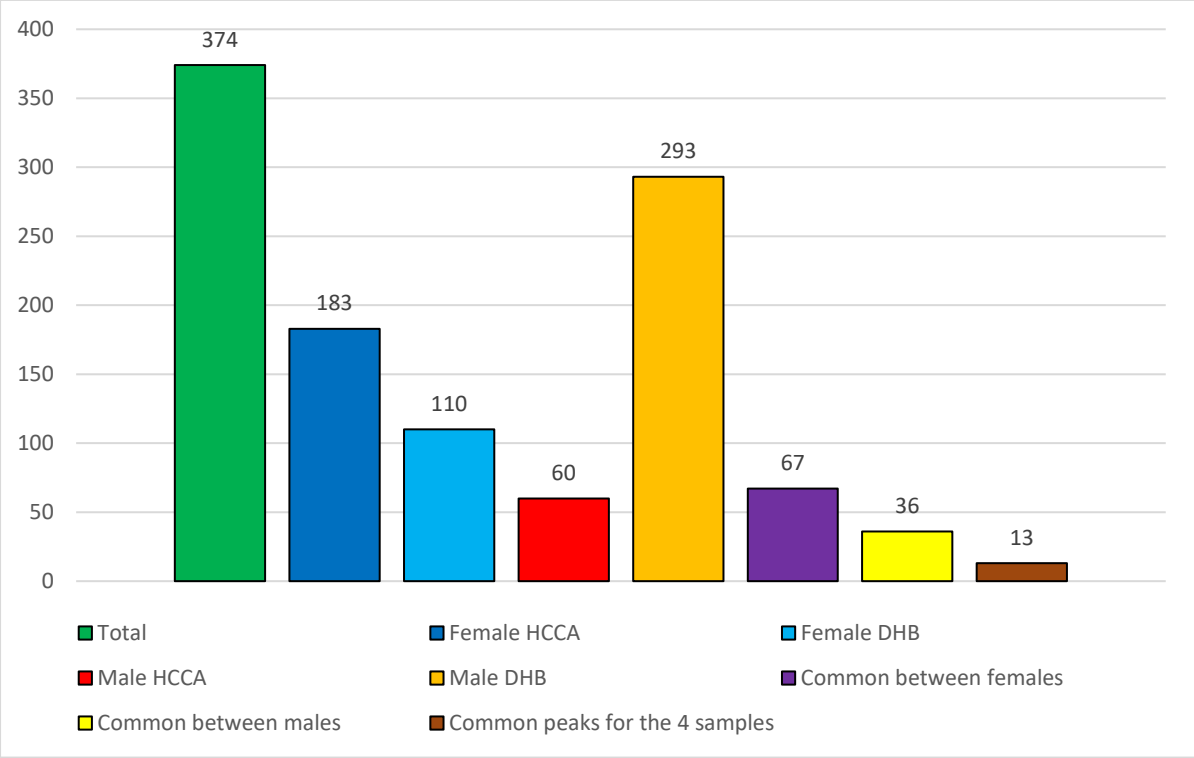

Figure 27. Histogram of the quantity of peaks for, in order: the total number detected, the peaks found for the female recovered with HCCA matrix, the peaks found for the female recovered with DHB matrix, the peaks found for the male recovered with HCCA matrix, the peaks found for the male recovered with DHB matrix, the peaks in common between the female samples, the peaks in common between the male samples and the peaks in common between all male and female samples.

In the case of the MSI experiments on the female *Steatoda nobilis* with HCCA matrix and the male with DHB matrix, since many zones are visible and since many families have been identified, this data can be subdivided to try to find patterns.

For the female sample, seven clear zones are visible: the nervous system, the brain, the vascular system, the eyes, the ovaries, the heart, and the silk glands (Figure 29). However, the molecules

[5] Master thesis supplementary information.docx

present can be subdivided into two other zones, the molecules that are present in both the nervous system and the brain, and the molecules present in any other zones which are not interesting to detail. The majority of the molecules are separated into these zones, but we can see in Figure 29 that the ovaries and the brain contain a large variety of molecules compared to the other zones.

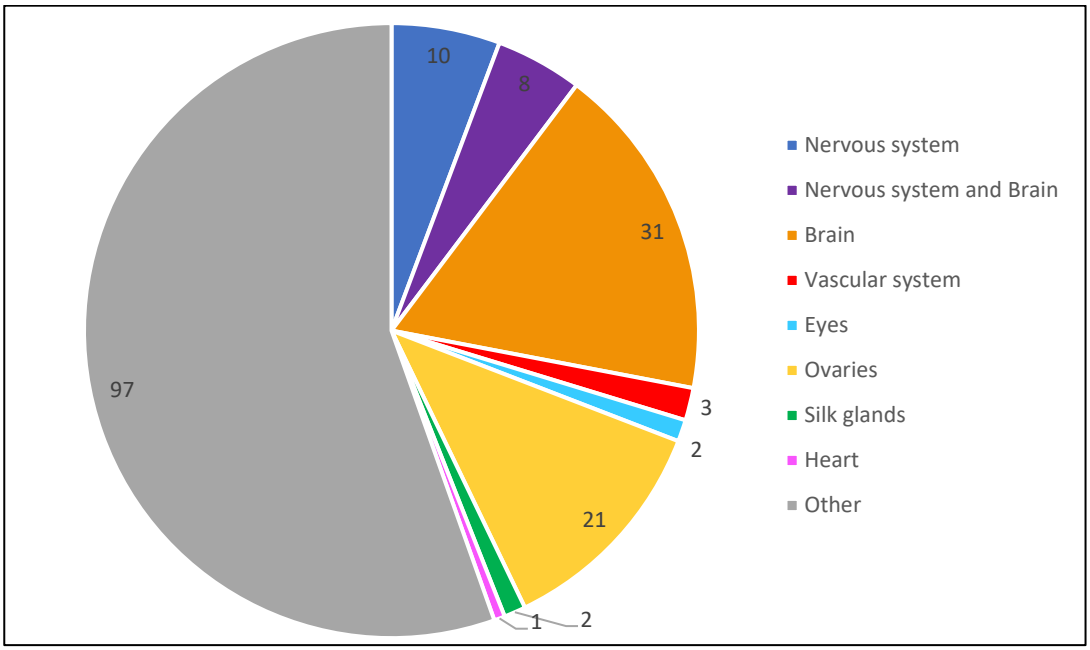

Figure 29. Pie chart of the number of molcules found in each zone for the MSI experiment of the female Steatoda nobilis with HCCA matrix. The “other” catergory means any other zone that was not noteworthy to mention.

Figure 30 details which kinds of molecules are detected in each zone. What stands out from this figure is the difference in the type of molecules present in the ovaries and the brain. There are only three families identified in the brain, while there are 3 identified families plus some other molecules in the ovaries. There seems to be a more complex mixture of molecules in the ovaries than in any other zone, which is not surprising considering oocytes and eggs are in development in this region.

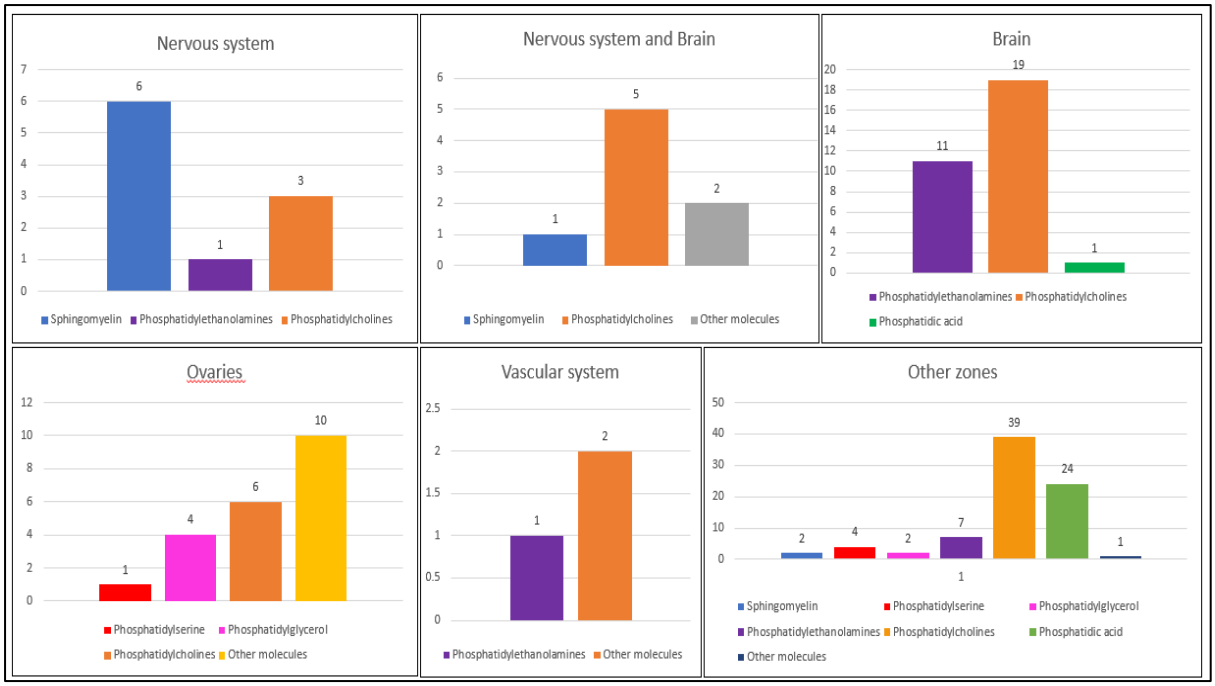

Figure 30. Histogram of the localization of families of molcules found in each zone for the MSI experiment of the female Steatoda nobilis with HCCA matrix. The "other zone" catergory means any other zone that was not noteworthy to mention. The "other molecules" catergory means any other molecules that were not present in enough numbers to be notewrothy.

Another interesting piece of information is in Figure 31, where the main families of molecules are represented. We can see that phosphatidylcholines and phosphatidylethanolamines are the two main families found for this sample and that they are mainly located in the brain and the ovaries.

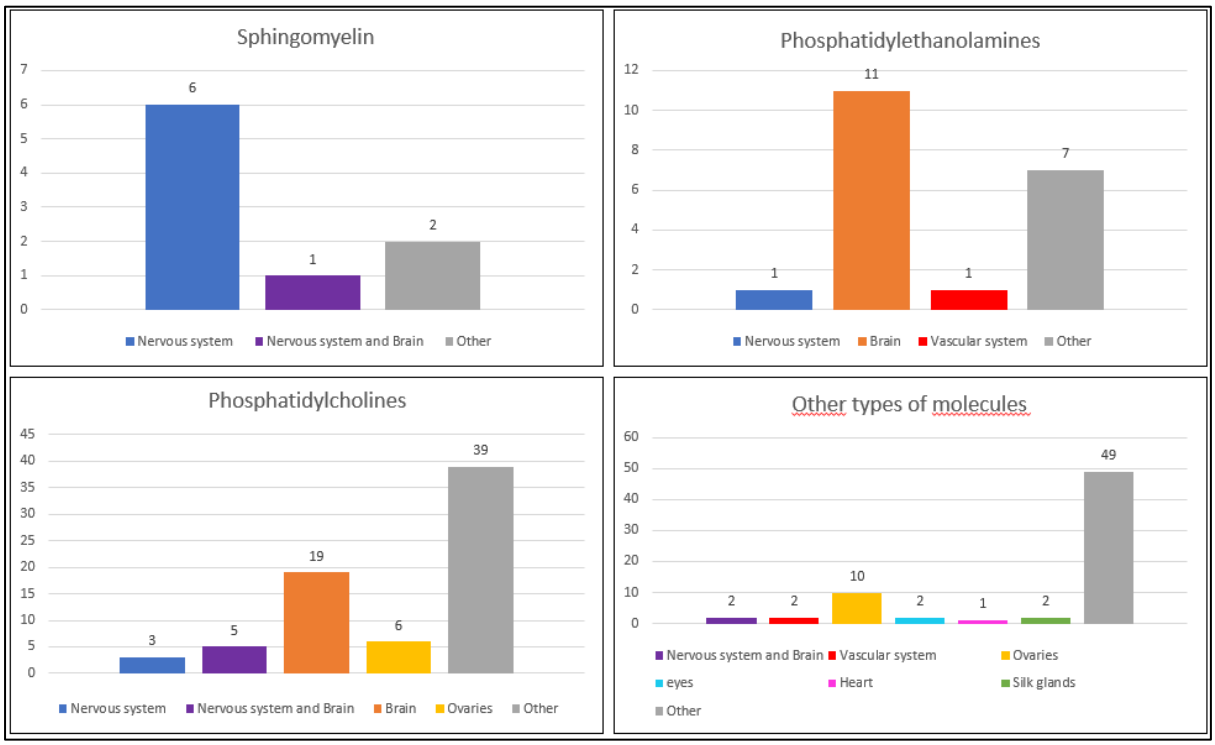

Figure 31. Histogram of the localization of families of molcules found in each zone for the MSI experiment of the female Steatoda nobilis with HCCA matrix. The "other" catergory means any other zone that was not noteworthy to mention. The "other molecules" catergory means any other molecules that were not present in enough numbers to be notewrothy.

For the male sample, there are fewer interesting zones to mention, only 3 zones are worth mentioning: the brain, the vascular system and zone combined zone of the nervous system and the brain when molecules are in common to both on the images. If we look at the molecules present per zone (Figure 33), the most interesting information is that sphingomyelins are present in the brain and in the nervous system. Like discussed above, sphingomyelins are components of myelin sheaths which surround nervous cells. It is therefore logical to find them in the nervous system and the brain and it also confirms the identification of these molecules.
In Figure 32 shows however that a lot of different molecules could detected in these zones, especially compared to the female samples. In short, female samples contain more interesting histological zones than males, but less molecules attributed to each zone could be identified. This could be due to the sectioning plane of the spider, since it is complicated to cut every spider at the exact same place, the difference between the two cutting planes can mean some organs are not visible in the section. The reason for that might lie in Figure 34, because way more phosphatidylcholines and phosphatidylethanolamines could be identified from male samples. Since these two families are the most present for both samples, the difference in the quantity of molecules per family might explain why the male sample has zones with more attributed analytes.

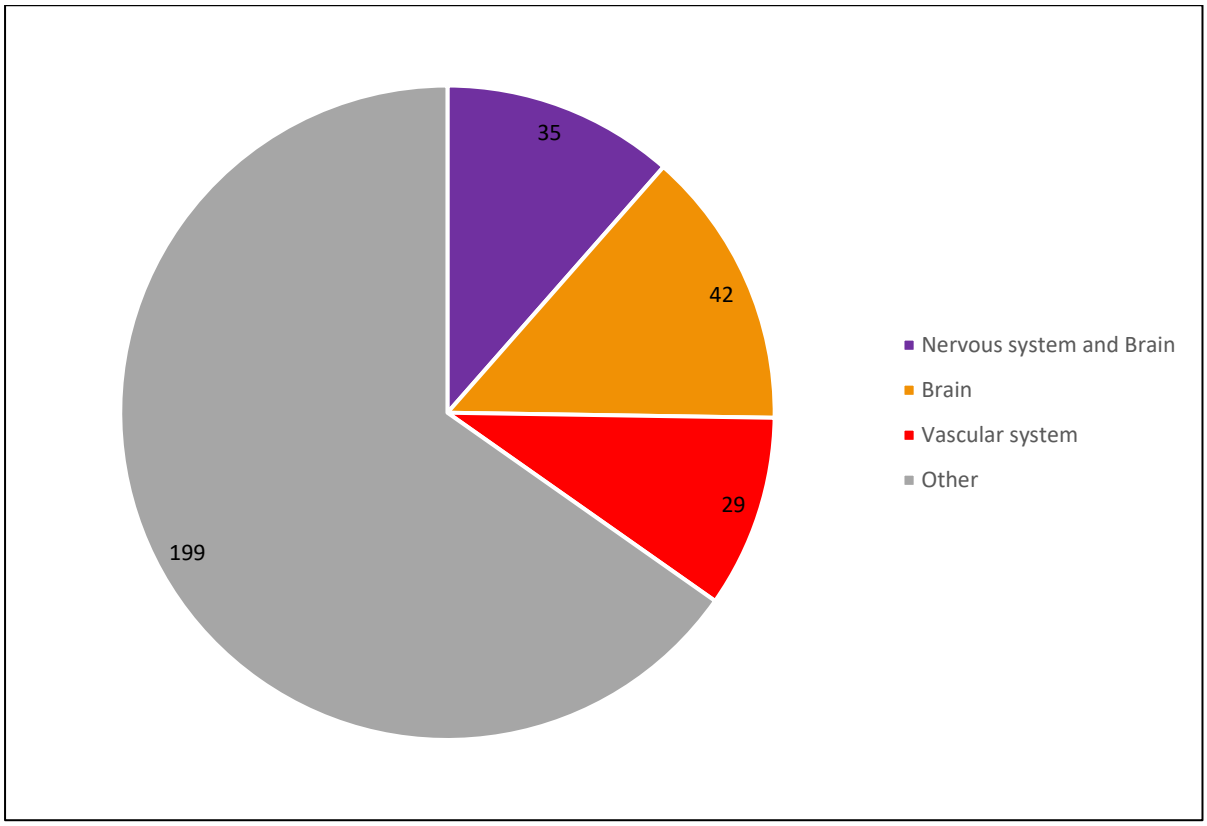

Figure 32. Pie chart of the number of molcules found in each zone for the MSI experiment of the male Steatoda nobilis with DHB matrix. The “other” catergory means any other zone that was not noteworthy to mention.

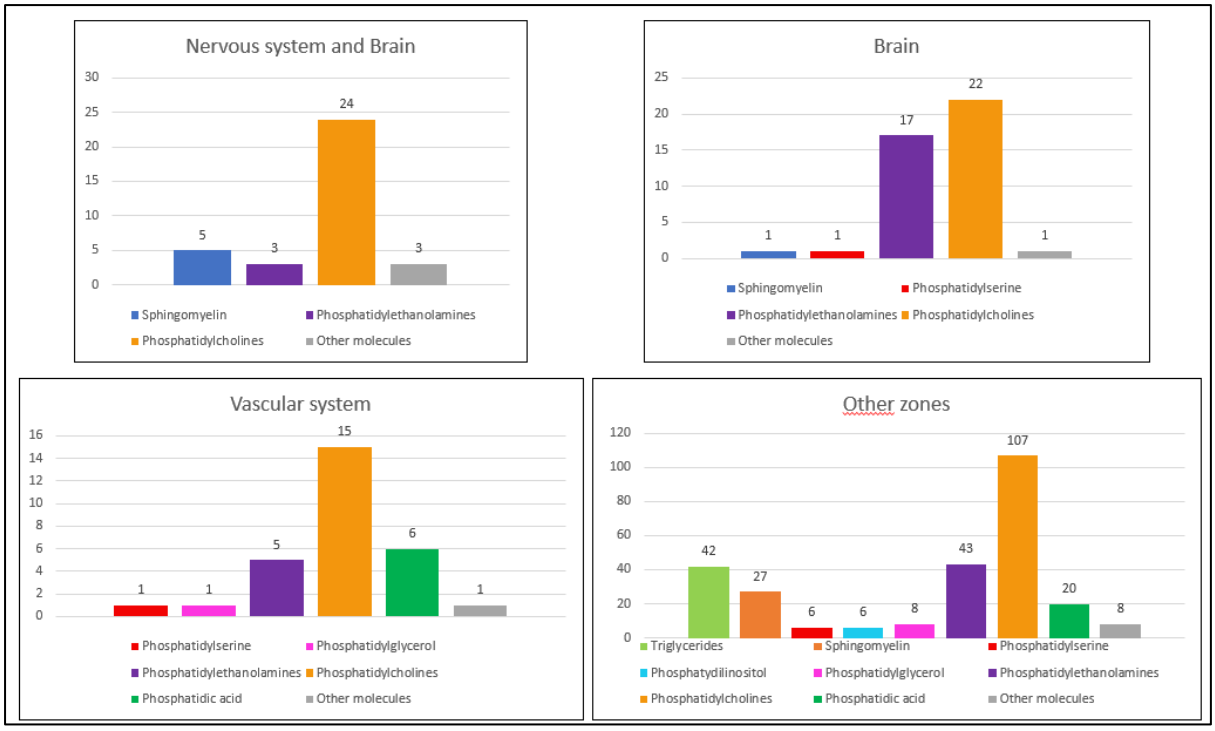

Figure 33. Histogram of the localization of families of molcules found in each zone for the MSI experiment of the male Steatoda nobilis with DHB matrix. The “other zone” catergory means any other zone that was not noteworthy to mention. The “other molecules” catergory means any other molecules that were not present in enough numbers to be notewrothy.

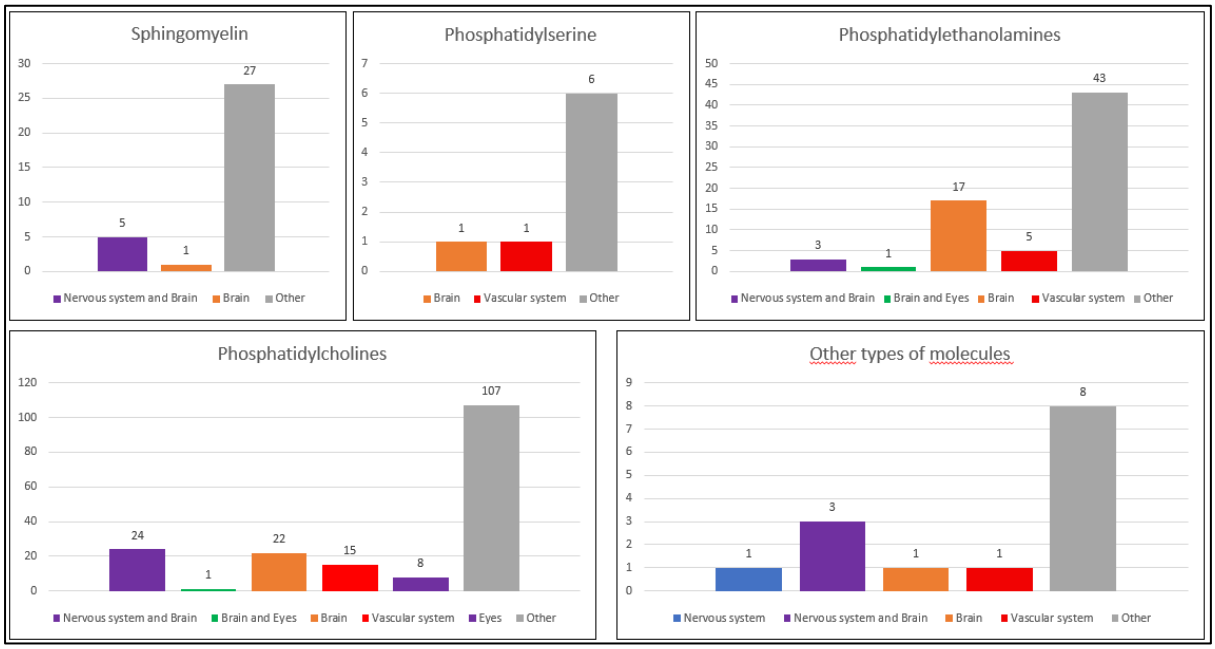

Figure 34. Histogram of the localization of families of molcules found in each zone for the MSI experiment of the male Steatoda nobilis with DHB matrix. The “other” catergory means any other zone that was not noteworthy to mention. The “other molecules” catergory means any other molecules that were not present in enough numbers to be notewrothy.

III. Synthesis of the results with all the techniques combined.

The analysis was performed on male and female *Steatoda nobilis* with 2 different matrices. An interesting result is that a large proportion of the molecules identified come from various families of metabolites, and especially lipids (like for example PC, phosphatidic acids(PA), phosphatidylethanolamines (PE) and triglycerides (TG)), although they are located in different zones. This means that even though some molecules are from the same family, some specific isoforms or isomers with a specific mass are only found in a specific zone of the sample. If a particular ion beloging to a family is detected in the brain and another one from the same family in the vascular system, their associated molecules may play different roles due to their specific mass and/or conformation. It is however impossible to determine their exact role only based on their identification, their m/z and their location. To understand the role they play, another analysis has to be made specifically to that purpose which is outside the scope of this study.

For the female samples, ten different zones can be seen for the slices covered with HCCA while only four can be seen for the one with DHB, which might suggest HCCA is a better matrix than DHB. But, for the male sample, five unclear zones (for example we can see if an ion is in the abdomen but we cannot pinpoint the exact organ or system it belongs to) can be seen for the samples covered with HCCA while seven more precise zones can be seen for the one with DHB. This means the matrix nature might not play a role in the details that can be seen in the images. However, since the spatial resolution is almost the same for all images (50 µm) but the male spiders are smaller to the females, the resolution of the images is higher for the female samples. Samples that are smaller led to lower resolutions in the images which could lead to a lack of spatial information. Ideally, for the current mass spectrometers in the lab, it seems that the spiders have to be a minimum of one centimeter long to obtain sufficient resolution for organs to be clearly separated from the rest in the analysis. With the current instruments, the spatial resolution power is not sufficient to have a clear image of the male, but in the future, the intsruments will keep getting better and the spatial resolution will probably improve significantly, at which point the minimum size of the sample will greatly decrease.

If we look at the differences between male and female with the same matrix, we can see that 18.9 % of the peaks are common between male and female covered in HCCA matrix while 33.0 % of the peaks are common between the two for the samples covered in DHB matrix. There are also 65.8 % more peaks for the DHB imaging runs than for the HCCA imaging runs. This suggests that the DHB has more reproducible results and that the ionization of the molecules in the sample is more effective. Be as it may, DHB also has a major disadvantage: the adducts formed by the matrix pollutes the MS spectra up to around 600 m/z compared to 200 m/z with HCCA. This means that very low weight molecules cannot be seen. But over that limit, only molecules coming from large families are identified, so information on smaller molecules not belonging to large families are lost.

Efforts to pinpoint the precise isomer through the utilization of MS/MS spectra proved unsuccessful, attributable to the previously outlined challenges. Within the appended data tables (supplementary information tables 2-5), when a molecule is denoted as identified, it signifies the successful identification of all isomeric variants of that particular molecule. Consequently, only the primary representatives from the respective molecular families are delineated in the table, streamlining the presentation for clarity and conciseness. One of the reason of this lack of success is the method used, indeed, since the images were aquired in non targeted mode, which means that the analysis cannot be aimed at finding a specific molecule. This explains why most MSI methods either concentrate on

small zones or target specific molecules instead of performing whole-body untargeted analysis. This problem will probably be resolved once MS/MS databases are more complete, because the identification will become easier once the fragmentation pattern of large quantities of molecules will be accessible for the analysis.

In MSI, the matrix and the way it is sprayed on samples, plays an important role in which molecules can be seen and in the reproducibility of the results. For arthropod metabolomics, the results of this analysis shows it is more important to detect very low mass molecules than having more reproducible results, as the higher mass molecules detected (>500 m/z) are part of large families which carry less interesting information.

V. Conclusion and perspective

During this master thesis we have performed the very first investigation of the metabolome of *Steatoda nobilis* using LC-MS/MS and MSI. The sample preparation was optimized to avoid any contamination during the LC-MS/MS but also to obtain better results in MSI. The LC-MS/MS provided information about the sample complexity, but also about the nature of the extracted molecules through their retention times, their masses and also their fragmentation pattern. The use of reversed phase and positive ionization only limits the detection of particular families of compounds, but solutions such as HILIC® and negative ionization mode exist to give our approach a more exhaustive profile. HILIC® is a type of column that separates molecules based on their polarity and that is usually opposed to reverse phase in metabolomics. This allows to see very polar molecules and changes the way the analytes are separated prior to the analysis which might impact the results. HILIC® can also be used as an additional separation step. The molecules, especially lipids, can be separated based on their polar head in HILIC®, then collected separately before being sent in a reverse-phase LC, prior to the mass spectrometer, to separate the molecules based on their hydrophobic parts. The main interest with negative ionization mode is that certain families of molecules, like …, cannot be seen in positive ionization mode (Dettmer *et al.*, 2007). Therefore, performing analysis in negative ionization mode can bring more information and uncover new zones on the sample studied.

The images obtained in MSI showed many different organs or zones of *Steatoda nobilis* that can be linked to histological sections to identify them, at the molecular level. These results suggest the presence of metabolites specific to these organs and probably linked to their biological function. Identification based on their exact masses can also be proposed due to the exact mass provided by the FT-ICR mass spectrometer, but isobar compounds could not be distinguished by this approach only. The data was processed using a trio of software composed by SCiLS®, MSKF and Metaspace®. The results that were thoroughly treated show that specific molecules or families can be detected in certain organs of the spider. The identification for the analytes can be obtained with Metaspace®, and research based for instance on the MS/MS fragmentation spectra can confirm the identification. The fragmentation spectra can be processed using MZmine 3®, which helps visualize the data and provides a comparison with spectral libraries, but the software is currently unable to treat the MS/MS data of the TIMSTOF-pro-2. This will hopefully change in the future and will bring new information for this kind of analysis. The combination of all the information from the software allows for an in-detail analysis of the images and seems to be the best processing method for MALDI MSI data. As discussed in the thesis, we must remind that the size of the MSI files that are generated for each image is a constraint, which require powerful computing power to correctly analyse. The lack of furnished databases, which renders the identification more complex and might lead to misidentification, is a second limitation.

Globally, this thesis allowed the identification of a large number of molecules present in *Steatoda nobilis* extracts, as well as their spatial distribution on the sections. This shows the potential of LC-MS/MS coupled to Mass spectrometry imaging for the metabolomic analysis of other arthropods and leads the path to other research that will be using the same method. The protocol for the sample preparation can be the same for any arthropods. Although the technique has been optimized for *Steatoda nobilis* but might require some adaptations for other species. If new studies are performed, this will resolve the problem of databases being incomplete and since computers keep getting better, since software are more and more advanced and since instruments are more and more powerful, the problem of the size of the files will disappear in the future.

VI. Bibliography

Acunha, T., Rocha, B. A., Nardini, V., Barbosa, F., & Faccioli, L. H. (2023). Lipidomic profiling of the Brazilian yellow scorpion venom: new insights into inflammatory responses following Tityus serrulatus envenomation. *Journal of Toxicology and Environmental Health - Part A: Current Issues*, *86*(9), 283–295. https://doi.org/10.1080/15287394.2023.2188896

Ahamad, J., Ali, F., Sayed, M. A., Ahmad, J., & Nollet, L. M. L. (2022). Basic Principles and Fundamental Aspects of Mass Spectrometry. In *Mass Spectrometry in Food Analysis* (pp. 3–17). CRC Press. https://doi.org/10.1201/9781003091226-2

Angerer, T. B., Bour, J., Biagi, J. L., Moskovets, E., & Frache, G. (2022). Evaluation of 6 MALDI-Matrices for 10 µm Lipid Imaging and On-Tissue MSn with AP-MALDI-Orbitrap. *Journal of the American Society for Mass Spectrometry*, *33*(5), 760–771. https://doi.org/10.1021/jasms.1c00327

Avela, H. F., & Sirén, H. (2020). Advances in lipidomics. In *Clinica Chimica Acta* (Vol. 510, pp. 123–141). Elsevier B.V. https://doi.org/10.1016/j.cca.2020.06.049

Awad, H., Khamis, M. M., & El-Aneed, A. (2015). Mass spectrometry, review of the basics: Ionization. In *Applied Spectroscopy Reviews* (Vol. 50, Issue 2, pp. 158–175). Bellwether Publishing, Ltd. https://doi.org/10.1080/05704928.2014.954046

Bales, J. R., Higham, D. P., Howe, I., Nicholson, J. K., & Sadler, P. J. (1984). Use of High-Resolution Proton Nuclear Magnetic Resonance Spectroscopy for Rapid Multi-Component Analysis of Urine. In *CLINICAL CHEMISTRY* (Vol. 30, Issue 3). https://academic.oup.com/clinchem/article-abstract/30/3/426/5668504

Bauer, T., Feldmeier, S., Krehenwinkel, H., Wieczorrek, C., Reiser, N., & Breitling, R. (2019). Steatoda nobilis, a false widow on the rise: A synthesis of past and current distribution trends. *NeoBiota*, *42*, 19–43. https://doi.org/10.3897/neobiota.42.31582

Becker, J. S., & Jakubowski, N. (2009). The synergy of elemental and biomolecular mass spectrometry: New analytical strategies in life sciences. *Chemical Society Reviews*, *38*(7), 1969–1983. https://doi.org/10.1039/b618635c

Bleiholder, C., Suhai, S., & Paizs, B. (2006). Revising the Proton Affinity Scale of the Naturally Occurring α-Amino Acids. *Journal of the American Society for Mass Spectrometry*, *17*(9), 1275–1281. https://doi.org/10.1016/j.jasms.2006.05.010

Boesl, U. (2017). Time-of-flight mass spectrometry: Introduction to the basics. In *Mass Spectrometry Reviews* (Vol. 36, Issue 1, pp. 86–109). John Wiley and Sons Inc. https://doi.org/10.1002/mas.21520

Boldin, I. A., & Nikolaev, E. N. (2011). Fourier transform ion cyclotron resonance cell with dynamic harmonization of the electric field in the whole volume by shaping of the excitation and detection electrode assembly. *Rapid Communications in Mass Spectrometry*, *25*(1), 122–126. https://doi.org/10.1002/rcm.4838

Brown, S. C., Kruppa, G., & Dasseux, J. L. (2005). Metabolomics applications of FT-ICR mass spectrometry. In *Mass Spectrometry Reviews* (Vol. 24, Issue 2, pp. 223–231). https://doi.org/10.1002/mas.20011

Caprioli Richard M., Farmer Terry B., & and Gile Jocelyn. (1997). Molecular Imaging of Biological Samples: Localization of Peptides and Proteins Using MALDI-TOF MS. In *Rapid Commun. Mass Spectrom* (Vol. 78, Issue 2). https://pubs.acs.org/sharingguidelines

Cech, N. B., & Enke, C. G. (2001). Practical implications of some recent studies in electrospray ionization fundamentals. *Mass Spectrometry Reviews*, *20*(6), 362–387. https://doi.org/10.1002/mas.10008

Challen, B., & Cramer, R. (2022). Advances in ionisation techniques for mass spectrometry-based omics research. In *Proteomics* (Vol. 22, Issues 15–16). John Wiley and Sons Inc. https://doi.org/10.1002/pmic.202100394

Chen, M., Blum, D., Engelhard, L., Raunser, S., Wagner, R., & Gatsogiannis, C. (2021). Molecular architecture of black widow spider neurotoxins. *Nature Communications*, *12*(1). https://doi.org/10.1038/s41467-021-26562-8

Chernushevich, I. V., Loboda, A. V., & Thomson, B. A. (2001). An introduction to quadrupole-time-of-flight mass spectrometry. *Journal of Mass Spectrometry*, *36*(8), 849–865. https://doi.org/10.1002/jms.207

D'Atri, V., Causon, T., Hernandez-Alba, O., Mutabazi, A., Veuthey, J. L., Cianferani, S., & Guillarme, D. (2018). Adding a new separation dimension to MS and LC–MS: What is the utility of ion mobility spectrometry? In *Journal of Separation Science* (Vol. 41, Issue 1, pp. 20–67). Wiley-VCH Verlag. https://doi.org/10.1002/jssc.201700919

Dettmer, K., Aronov, P. A., & Hammock, B. D. (2007). Mass spectrometry-based metabolomics. In *Mass Spectrometry Reviews* (Vol. 26, Issue 1, pp. 51–78). https://doi.org/10.1002/mas.20108

Dole, M., Mack, L. L., Hines, R. L., Chemistry, D. O., Mobley, R. C., Ferguson, L. D., & Alice, M. B. (1968). Molecular beams of macroions. *The Journal of Chemical Physics*, *49*(5), 2240–2249. https://doi.org/10.1063/1.1670391

Dreisbach, D., Bhandari, D. R., Betz, A., Tenbusch, L., Vilcinskas, A., Spengler, B., & Petschenka, G. (2023). Spatial metabolomics reveal divergent cardenolide processing in the monarch (*Danaus plexippus*) and the common crow butterfly (*Euploea core*). *Molecular Ecology Resources*. https://doi.org/10.1111/1755-0998.13786

Dugon, M. M., Dunbar, J. P., Afoullouss, S., Schulte, J., McEvoy, A., English, M. J., Hogan, R., Ennis, C., & Sul, R. (2017). Occurrence, reproductive rate and identification of the non-native noble false widow spider steatoda nobilis (thorell, 1875) in Ireland. *Biology and Environment*, *117B*(2), 77–89. https://doi.org/10.3318/BIOE.2017.11

Dugon, M. M., Lawton, C., Sturgess, D., & Dunbar, J. P. (2023). Predation on a pygmy shrew, *Sorex minutus* , by the noble false widow spider, *Steatoda nobilis*. *Ecosphere*, *14*(2). https://doi.org/10.1002/ecs2.4422

Dunbar, J. P., Fort, A., Redureau, D., Sulpice, R., Dugon, M. M., & Quinton, L. (2020). Venomics approach reveals a high proportion of lactrodectus-like toxins in the venom of the noble falsewidow spider steatoda nobilis. *Toxins*, *12*(6). https://doi.org/10.3390/toxins12060402

Dunbar, J. P., Vitkauskaite, A., Lawton, C., Waddams, B., & Dugon, M. M. (2022). Webslinger vs. Dark Knight First record of a false widow spider Steatoda nobilis preying on a pipistrelle bat in Britain. *Ecosphere*, *13*(2). https://doi.org/10.1002/ecs2.3959

Dunbar, J. P., Vitkauskaite, A., O'Keeffe, D. T., Fort, A., Sulpice, R., & Dugon, M. M. (2022a). Bites by the noble false widow spider Steatoda nobilis can induce Latrodectus-like symptoms and vector-borne bacterial infections with implications for public health: a case series. *Clinical Toxicology*, *60*(1), 59–70. https://doi.org/10.1080/15563650.2021.1928165

Dunbar, J. P., Vitkauskaite, A., O'Keeffe, D. T., Fort, A., Sulpice, R., & Dugon, M. M. (2022b). Clinical evidence of necrosis following bites by the Noble false widow spider Steatoda nobilis–a response to Paolino & colleagues. In *Clinical Toxicology* (Vol. 60, Issue 2, pp. 276–277). Taylor and Francis Ltd. https://doi.org/10.1080/15563650.2021.1955130

El-Aneed, A., Cohen, A., & Banoub, J. (2009). Mass spectrometry, review of the basics: Electrospray, MALDI, and commonly used mass analyzers. In *Applied Spectroscopy Reviews* (Vol. 44, Issue 3, pp. 210–230). https://doi.org/10.1080/05704920902717872

Fenn John B, & Yamashitat Masamichi. (1984). Electrospray Ion Source. Another Variation on the Free-Jet Theme. *American Chemical Society*.

Gao, S. Q., Zhao, J. H., Guan, Y., Tang, Y. S., Li, Y., & Liu, L. Y. (2022). Mass spectrometry imaging technology in metabolomics: A systematic review. In *Biomedical Chromatography*. John Wiley and Sons Ltd. https://doi.org/10.1002/bmc.5494

Ghezellou, P., Jakob, K., Atashi, J., Ghassempour, A., & Spengler, B. (2022). Mass-Spectrometry-Based Lipidome and Proteome Profiling of Hottentotta saulcyi (Scorpiones: Buthidae) Venom. *Toxins*, *14*(6). https://doi.org/10.3390/toxins14060370

Gomez, A., & Tang, K. (1994). Charge and fission of droplets in electrostatic sprays. *Physics of Fluids*, *6*(1), 404–414. https://doi.org/10.1063/1.868037

Goñi, F. M. (2022). Sphingomyelin: What is it good for? In *Biochemical and Biophysical Research Communications* (Vol. 633, pp. 23–25). Elsevier B.V. https://doi.org/10.1016/j.bbrc.2022.08.074

Griffiths, J. (2008). A brief history of mass spectrometry. In *Analytical Chemistry* (Vol. 80, Issue 15, pp. 5678–5683). https://doi.org/10.1021/ac8013065

Gutiérrez, Y., Fresch, M., Scherber, C., & Brockmeyer, J. (2022). The lipidome of an omnivorous insect responds to diet composition and social environment. *Ecology and Evolution*, *12*(11). https://doi.org/10.1002/ece3.9497

He, M. J., Pu, W., Wang, X., Zhang, W., Tang, D., & Dai, Y. (2022). Comparing DESI-MSI and MALDI-MSI Mediated Spatial Metabolomics and Their Applications in Cancer Studies. In *Frontiers in Oncology* (Vol. 12). Frontiers Media S.A. https://doi.org/10.3389/fonc.2022.891018

Heiles, S. (2021). Advanced tandem mass spectrometry in metabolomics and lipidomics-methods and applications. *Analytical and Bioanalytical Chemistry*. https://doi.org/10.1007/s00216-021-03425-1/Published

Herbert, C. G., & Johnstone, R. A. W. (Robert A. W. (2003). *Mass spectrometry basics*. CRC Press.

Horvath, T. D., Dagan, S., & Scaraffia, P. Y. (2021). Unraveling mosquito metabolism with mass spectrometry-based metabolomics. In *Trends in Parasitology* (Vol. 37, Issue 8, pp. 747–761). Elsevier Ltd. https://doi.org/10.1016/j.pt.2021.03.010

Hosseini, S., & Martinez-Chapa, S. O. (2017). Principles and mechanism of MALDI-ToF-MS analysis. In *SpringerBriefs in Applied Sciences and Technology* (Issue 9789811023552, pp. 1–19). Springer Verlag. https://doi.org/10.1007/978-981-10-2356-9_1

Hustin, J., Kune, C., Far, J., Eppe, G., Debois, D., Quinton, L., & De Pauw, E. (2022). Differential Kendrick's plots as an innovative tool for lipidomics in complex samples: comparison of liquid chromatography and infusion-based methods to sample differential study. *American Chemical Society*. www.lipidmaps.org

Jacob, M., Lopata, A. L., Dasouki, M., & Abdel Rahman, A. M. (2019). Metabolomics toward personalized medicine. In *Mass Spectrometry Reviews* (Vol. 38, Issue 3, pp. 221–238). John Wiley and Sons Inc. https://doi.org/10.1002/mas.21548

Jaskolla, T. W., & Karas, M. (2011). Compelling evidence for lucky survivor and gas phase protonation: The unified MALDI analyte protonation mechanism. *Journal of the American Society for Mass Spectrometry*, *22*(6), 976–988. https://doi.org/10.1007/s13361-011-0093-0

Jimenez, E. C., Olivera, B. M., & Teichert, R. W. (2007). αC-conotoxin PrXA: A new family of nicotinic acetylcholine receptor antagonists. *Biochemistry*, *46*(30), 8717–8724. https://doi.org/10.1021/bi700582m

Karas, M., Bachmann, D., Bahr, U., & Hillenkamp, F. (1987). Matrix-assisted ultraviolet laser desorption of non-volatile compounds. *International Journal of Mass Spectrometry and Ion Processes*, *78*, 53–68. https://doi.org/10.1016/0168-1176(87)87041-6

Karas, M., Bachmann, D., & Hillenkamp, F. (1985a). Influence of the Wavelength in High-Irradiance Ultraviolet Laser Desorption Mass Spectrometry of Organic Molecules. In *Anal. Chem* (Vol. 57).

Karas, M., Bachmann, D., & Hillenkamp, F. (1985b). Influence of the Wavelength in High-Irradiance Ultraviolet Laser Desorption Mass Spectrometry of Organic Molecules. In *Anal. Chem* (Vol. 57).

Karas, M., Glückmann, M., & Schäfer, J. (2000). Ionization in matrix-assisted laser desorption/ionization: Singly charged molecular ions are the lucky survivors. *Journal of Mass Spectrometry*, *35*(1), 1–12. https://doi.org/10.1002/(SICI)1096-9888(200001)35:1<1::AID-JMS904>3.0.CO;2-0

Karger, A., Kampen, H., Bettin, B., Dautel, H., Ziller, M., Hoffmann, B., Süss, J., & Klaus, C. (2012). Species determination and characterization of developmental stages of ticks by whole-animal matrix-assisted laser desorption/ionization mass spectrometry. *Ticks and Tick-Borne Diseases*, *3*(2), 78–89. https://doi.org/10.1016/j.ttbdis.2011.11.002

Kebarle, P. (2000). A brief overview of the present status of the mechanisms involved in electrospray mass spectrometry. In *Journal of Mass Spectrometry* (Vol. 35, Issue 7, pp. 804–817). https://doi.org/10.1002/1096-9888(200007)35:7<804::AID-JMS22>3.0.CO;2-Q

Kendrick, E. (1963). A Mass Scale Based on CH,= 14.0000 for High Resolution Mass Spectrometry of Organic Compounds. *American Chemical Society*.

Kicman, A. T., Parkin, M. C., & Iles, R. K. (2007). An introduction to mass spectrometry based proteomics-Detection and characterization of gonadotropins and related molecules. In *Molecular and Cellular Endocrinology* (Vols. 260–262, pp. 212–227). https://doi.org/10.1016/j.mce.2006.02.022

Klupczynska, A., Pawlak, M., Kokot, Z. J., & Matysiak, J. (2018). Application of metabolomic tools for studying low molecular-weight fraction of animal venoms and poisons. In *Toxins* (Vol. 10, Issue 8). MDPI AG. https://doi.org/10.3390/toxins10080306

Knochenmuss, R., Stortelder, A., Breuker, K., & Zenobi, R. (2000). Secondary ion-molecule reactions in matrix-assisted laser desorption/ionization. *Journal of Mass Spectrometry*, *35*(11), 1237–1245. https://doi.org/10.1002/1096-9888(200011)35:11<1237::AID-JMS74>3.0.CO;2-O

Knochenmuss, R., & Zenobi, R. (2003). MALDI ionization: The role of in-plume processes. *Chemical Reviews*, *103*(2), 441–452. https://doi.org/10.1021/cr0103773

Konermann, L., Ahadi, E., Rodriguez, A. D., & Vahidi, S. (2013). Unraveling the mechanism of electrospray ionization. *Analytical Chemistry*, *85*(1), 2–9. https://doi.org/10.1021/ac302789c

Lemaire, R., Tabet, J. C., Ducoroy, P., Hendra, J. B., Salzet, M., & Fournier, I. (2006). Solid ionic matrixes for direct tissue analysis and MALDI imaging. *Analytical Chemistry*, *78*(3), 809–819. https://doi.org/10.1021/ac0514669

Lemaire, R., Wisztorski, M., Desmons, A., Tabet, J. C., Day, R., Salzet, M., & Fournier, I. (2006). MALDI-MS direct tissue analysis of proteins: Improving signal sensitivity using organic treatments. *Analytical Chemistry*, *78*(20), 7145–7153. https://doi.org/10.1021/ac060565z

Leopold, J., Popkova, Y., Engel, K. M., & Schiller, J. (2018). Recent developments of useful MALDI matrices for the mass spectrometric characterization of lipids. In *Biomolecules* (Vol. 8, Issue 4). MDPI AG. https://doi.org/10.3390/biom8040173

Liu, H., Pan, Y., Xiong, C., Han, J., Wang, X., Chen, J., & Nie, Z. (2022). Matrix-assisted laser desorption/ionization mass spectrometry imaging (MALDI MSI) for in situ analysis of endogenous small molecules in biological samples. In *TrAC - Trends in Analytical Chemistry* (Vol. 157). Elsevier B.V. https://doi.org/10.1016/j.trac.2022.116809

Macnair, J. E., Lewis, K. C., & Jorgenson, J. W. (1997). Ultrahigh-Pressure Reversed-Phase Liquid Chromatography in Packed Capillary Columns A C R e s e a r c h. In *Analytical Chemistry* (Vol. 69, Issue 6). UTC. https://pubs.acs.org/sharingguidelines

Mainini, V., Lalowski, M., Gotsopoulos, A., Bitsika, V., Baumann, M., & Magni, F. (2015). Maldi-imaging mass spectrometry on tissues. *Methods in Molecular Biology*, *1243*, 139–164. https://doi.org/10.1007/978-1-4939-1872-0_8

Markert, C., Thinius, M., Lehmann, L., Heintz, C., Stappert, F., Wissdorf, W., Kersten, H., Benter, T., Schneider, B. B., & Covey, T. R. (2021). Observation of charged droplets from electrospray ionization (ESI) plumes in API mass spectrometers. *Analytical and Bioanalytical Chemistry*. https://doi.org/10.1007/s00216-021-03452-y/Published

McCann, A., Kune, C., La Rocca, R., Oetjen, J., Arias, A. A., Ongena, M., Far, J., Eppe, G., Quinton, L., & De Pauw, E. (2021). Rapid visualization of lipopeptides and potential bioactive groups of compounds by combining ion mobility and MALDI imaging mass spectrometry. In *Drug Discovery Today: Technologies* (Vol. 39, pp. 81–88). Elsevier Ltd. https://doi.org/10.1016/j.ddtec.2021.08.003

McDonnell, L. A., Heeren, R. M. A., de Lange, R. P. J., & Fletcher, I. W. (2006). Higher Sensitivity Secondary Ion Mass Spectrometry of Biological Molecules for High Resolution, Chemically Specific Imaging. *Journal of the American Society for Mass Spectrometry*, *17*(9), 1195–1202. https://doi.org/10.1016/j.jasms.2006.05.003

Meier, F., Beck, S., Grassl, N., Lubeck, M., Park, M. A., Raether, O., & Mann, M. (2015). Parallel accumulation-serial fragmentation (PASEF): Multiplying sequencing speed and sensitivity by synchronized scans in a trapped ion mobility device. *Journal of Proteome Research*, *14*(12), 5378–5387. https://doi.org/10.1021/acs.jproteome.5b00932

Meier, F., Brunner, A. D., Koch, S., Koch, H., Lubeck, M., Krause, M., Goedecke, N., Decker, J., Kosinski, T., Park, M. A., Bache, N., Hoerning, O., Cox, J., Räther, O., & Mann, M. (2018). Online parallel accumulation–serial fragmentation (PASEF) with a novel trapped ion mobility mass spectrometer. *Molecular and Cellular Proteomics*, *17*(12), 2534–2545. https://doi.org/10.1074/mcp.TIR118.000900

Meier, F., Park, M. A., & Mann, M. (2021). Trapped ion mobility spectrometry and parallel accumulation–serial fragmentation in proteomics. In *Molecular and Cellular Proteomics* (Vol. 20). American Society for Biochemistry and Molecular Biology Inc. https://doi.org/10.1016/j.mcpro.2021.100138

Mielczarek, P., Suder, P., Kret, P., Słowik, T., Gibuła-Tarłowska, E., Kotlińska, J. H., Kotsan, I., & Bodzon-Kulakowska, A. (2023). Matrix-assisted laser desorption/ionization mass spectrometry imaging sample preparation using wet-interface matrix deposition for lipid analysis. *Rapid Communications in Mass Spectrometry*, *37*(14). https://doi.org/10.1002/rcm.9531

Misra Gauri, Rajawat, J., & Jhingan, G. (2019). *Data processing handbook for complex biological data sources*.

Molnar, B. T., & Shelley, J. T. (2021). MODERN PLASMA-BASED DESORPTION/IONIZATION: FROM ATOMS AND MOLECULES TO CHEMICAL SYNTHESIS. In *Mass Spectrometry Reviews* (Vol. 40, Issue 5, pp. 609–627). John Wiley and Sons Inc. https://doi.org/10.1002/mas.21645

Müller, W. H., Verdin, A., De Pauw, E., Malherbe, C., & Eppe, G. (2022). Surface-assisted laser desorption/ionization mass spectrometry imaging: A review. In *Mass Spectrometry Reviews* (Vol. 41, Issue 3, pp. 373–420). John Wiley and Sons Inc. https://doi.org/10.1002/mas.21670

Myers, J., Grothaus, G., Narayanan, S., & Onufriev, A. (2006). A simple clustering algorithm can be accurate enough for use in calculations of pKs in macromolecules. *Proteins: Structure, Function and Genetics*, *63*(4), 928–938. https://doi.org/10.1002/prot.20922

Nagana Gowda, G. A., & Djukovic, D. (2014). Overview of mass spectrometry-based metabolomics: Opportunities and challenges. *Methods in Molecular Biology*, *1198*, 3–12. https://doi.org/10.1007/978-1-4939-1258-2_1

Nikolaev, E. N., Boldin, I. A., Jertz, R., & Baykut, G. (2011). Initial experimental characterization of a new ultra-high resolution FTICR cell with dynamic harmonization. *Journal of the American Society for Mass Spectrometry*, *22*(7), 1125–1133. https://doi.org/10.1007/s13361-011-0125-9

Norris, J. L., Cornett, D. S., Mobley, J. A., Andersson, M., Seeley, E. H., Chaurand, P., & Caprioli, R. M. (2007). Processing MALDI Mass Spectra to Improve Mass Spectral Direct Tissue Analysis. *Int J Mass Spectrom*.

Parrot, D., Papazian, S., Foil, D., & Tasdemir, D. (2018). Imaging the Unimaginable: Desorption Electrospray Ionization - Imaging Mass Spectrometry (DESI-IMS) in Natural Product Research. In *Planta Medica* (Vol. 84, Issues 9–10, pp. 584–593). Georg Thieme Verlag. https://doi.org/10.1055/s-0044-100188

Perez de Souza, L., Alseekh, S., Scossa, F., & Fernie, A. R. (2021). Ultra-high-performance liquid chromatography high-resolution mass spectrometry variants for metabolomics research. In *Nature Methods* (Vol. 18, Issue 7, pp. 733–746). Nature Research. https://doi.org/10.1038/s41592-021-01116-4

Perry, W. J., Patterson, N. H., Prentice, B. M., Neumann, E. K., Caprioli, R. M., & Spraggins, J. M. (2020). Uncovering matrix effects on lipid analyses in MALDI imaging mass spectrometry experiments. *Journal of Mass Spectrometry*, *55*(4). https://doi.org/10.1002/jms.4491

Plsonero, J., & Günther, D. (2008). Femtosecond laser ablation inductively coupled plasma mass spectrometry: Fundamentals and capabilities for depth profiling analysis. *Mass Spectrometry Reviews*, *27*(6), 609–623. https://doi.org/10.1002/mas.20180

Rayner, S., Vitkauskaite, A., Healy, K., Lyons, K., McSharry, L., Leonard, D., Dunbar, J. P., & Dugon, M. M. (2022). Worldwide Web: High Venom Potency and Ability to Optimize Venom Usage Make the Globally Invasive Noble False Widow Spider Steatoda nobilis (Thorell, 1875) (Theridiidae) Highly Competitive against Native European Spiders Sharing the Same Habitats. *Toxins*, *14*(9). https://doi.org/10.3390/toxins14090587

Ren, J. L., Zhang, A. H., Kong, L., & Wang, X. J. (2018). Advances in mass spectrometry-based metabolomics for investigation of metabolites. *RSC Advances*, *8*(40), 22335–22350. https://doi.org/10.1039/c8ra01574k

Ridgeway, M. E., Lubeck, M., Jordens, J., Mann, M., & Park, M. A. (2018). Trapped ion mobility spectrometry: A short review. In *International Journal of Mass Spectrometry* (Vol. 425, pp. 22–35). Elsevier B.V. https://doi.org/10.1016/j.ijms.2018.01.006

Saber, F. R., Abdelbary, G. A., Salama, M. M., Saleh, D. O., Fathy, M. M., & Soliman, F. M. (2018). UPLC/QTOF/MS profiling of two Psidium species and the in-vivo hepatoprotective activity of their nano-formulated liposomes. *Food Research International*, *105*, 1029–1038. https://doi.org/10.1016/j.foodres.2017.12.042

Scaraffia, P. Y., Zhang, Q., Wysocki, V. H., Isoe, J., & Wells, M. A. (2006). Analysis of whole body ammonia metabolism in Aedes aegypti using [15N]-labeled compounds and mass spectrometry. *Insect Biochemistry and Molecular Biology*, *36*(8), 614–622. https://doi.org/10.1016/j.ibmb.2006.05.003

Schwartz, S. A., Reyzer, M. L., & Caprioli, R. M. (2003). Direct tissue analysis using matrix-assisted laser desorption/ionization mass spectrometry: Practical aspects of sample preparation. *Journal of Mass Spectrometry*, *38*(7), 699–708. https://doi.org/10.1002/jms.505

Short, R. T., & Todd, P. J. (1994). *Improved Energy Compensation for Time-of-Flight Mass Spectrometry**.

Smith, A., Piga, I., Galli, M., Stella, M., Denti, V., del Puppo, M., & Magni, F. (2017). Matrix-assisted laser desorption/ionisation mass spectrometry imaging in the study of gastric cancer: A mini review. In *International Journal of Molecular Sciences* (Vol. 18, Issue 12). MDPI AG. https://doi.org/10.3390/ijms18122588

Snyder, L. R., & Kirkland, J. J. (Joseph J. (1979). *Introduction to modern liquid chromatography*. Wiley.

Tanaka, K. (1989). Energetic Cost of Web Construction and Its Effect on Web Relocation in the Web-Building Spider Agelena limbata. In *Source: Oecologia* (Vol. 81, Issue 4).

Tanaka Koichi, Waki Hiroaki, Ido Yutaka, Akita Satochi, Yoshida Yoshikazu, & Yoshida Tomio. (1988). Reactivity of N-Methylidenemalonates of 3-Arylaminoindoles and p-Dimethylamino-N-Phenylaniline in the Course of Their Analysis by Electrospray Ionization Mass Spectrometry. *International Journal of Analytical Mass Spectrometry and Chromatography*. https://doi.org/10.1002/rcm.1290020802

Tang, D. Q., Zou, L., Yin, X. X., & Ong, C. N. (2016). HILIC-MS for metabolomics: An attractive and complementary approach to RPLC-MS. In *Mass spectrometry reviews* (Vol. 35, Issue 5, pp. 574–600). John Wiley and Sons Inc. https://doi.org/10.1002/mas.21445

Tóth, F., Cseh, E. K., & Vécsei, L. (2021). Natural molecules and neuroprotection: Kynurenic acid, pantethine and α-lipoic acid. In *International Journal of Molecular Sciences* (Vol. 22, Issue 1, pp. 1–25). MDPI AG. https://doi.org/10.3390/ijms22010403

Vial, T., Tan, W.-L., Deharo, E., Missé, D., Marti, G., & Pompon, J. (2020). Mosquito metabolomics reveal that dengue virus replication requires phospholipid reconfiguration via the remodeling cycle. *Proceedings of the National Academy of Sciences of the United States of America*. https://doi.org/10.1073/pnas.2015095117/-/DCSupplemental

Wang, H. Y., Chu, X., Zhao, Z. X., He, X. S., & Guo, Y. L. (2011). Analysis of low molecular weight compounds by MALDI-FTICR-MS. In *Journal of Chromatography B: Analytical Technologies in the Biomedical and Life Sciences* (Vol. 879, Issues 17–18, pp. 1166–1179). https://doi.org/10.1016/j.jchromb.2011.03.037

Wang, M., & Marshall, A. G. (1988). High-Resolution Multiple-Ion Simultaneous Monitoring by Means of Multiple-Foldover Fourier Transform Ion Cyclotron Resonance Mass Spectrometry. In *Anal. Chem* (Vol. 60).

Wiesner, P., & Watson, K. E. (2017). Triglycerides: A reappraisal. In *Trends in Cardiovascular Medicine* (Vol. 27, Issue 6, pp. 428–432). Elsevier Inc. https://doi.org/10.1016/j.tcm.2017.03.004

Yan, S., & Wang, X. (2015). Recent advances in research on widow spider venoms and toxins. In *Toxins* (Vol. 7, Issue 12, pp. 5055–5067). MDPI AG. https://doi.org/10.3390/toxins7124862

Yang, F.-Y., He, W.-Y., & You, M.-S. (2020). Current Advances in Mass Spectrometry Imaging for Insect Physiology and Metabolism. In *Pests, Weeds and Diseases in Agricultural Crop and Animal Husbandry Production*. www.intechopen.com

Zangrando, R., Zanella, V., Karroca, O., Barbaro, E., Kehrwald, N. M., Battistel, D., Morabito, E., Gambaro, A., & Barbante, C. (2020). Dissolved organic matter in the deep TALDICE ice core: A nano-UPLC-nano-ESI-HRMS method. *Science of the Total Environment*, *700*. https://doi.org/10.1016/j.scitotenv.2019.134432